frontiers | Frontiers in Marine Science

TYPE Original Research
PUBLISHED 04 July 2023
DOI 10.3389/fmars.2023.1192242

Check for updates

OPEN ACCESS

EDITED BY
Elva G. Escobar-Briones,
National Autonomous University of Mexico, Mexico

REVIEWED BY
Jeroen Ingels,
Florida State University, United States
Jan Marcin Weslawski,
Polish Academy of Sciences, Poland

*CORRESPONDENCE
Henk-Jan Hoving
hhoving@geomar.de
Autun Purser
autun.purser@awi.de

RECEIVED 23 March 2023
ACCEPTED 12 June 2023
PUBLISHED 04 July 2023

CITATION
Hoving H-J, Boetius A, Dunlop K, Greinert J, Haeckel M, Jones DOB, Simon-Lledó E, Marcon Y, Stratmann T, Suck I, Sweetman AK and Purser A (2023) Major fine-scale spatial heterogeneity in accumulation of gelatinous carbon fluxes on the deep seabed.
Front. Mar. Sci. 10:1192242.
doi: 10.3389/fmars.2023.1192242

COPYRIGHT
© 2023 Hoving, Boetius, Dunlop, Greinert, Haeckel, Jones, Simon-Lledó, Marcon, Stratmann, Suck, Sweetman and Purser. This is an open-access article distributed under the terms of the Creative Commons Attribution License (CC BY). The use, distribution or reproduction in other forums is permitted, provided the original author(s) and the copyright owner(s) are credited and that the original publication in this journal is cited, in accordance with accepted academic practice. No use, distribution or reproduction is permitted which does not comply with these terms.

Major fine-scale spatial heterogeneity in accumulation of gelatinous carbon fluxes on the deep seabed

Henk-Jan Hoving[1]*, Antje Boetius[2,3,4], Katherine Dunlop[5], Jens Greinert[1,6], Matthias Haeckel[1], Daniel O. B. Jones[7], Erik Simon-Lledó[7], Yann Marcon[2], Tanja Stratmann[4,8,9], Inken Suck[1], Andrew K. Sweetman[10] and Autun Purser[3]*

[1]GEOMAR Helmholtz Centre for Ocean Research Kiel, Kiel, Germany, [2]MARUM – Center for Marine Environmental Sciences, University of Bremen, Bremen, Germany, [3]Alfred Wegener Institute Helmholtz Centre for Polar and Marine Research, Bremerhaven, Germany, [4]Max Planck Institute for Marine Microbiology, Bremen, Germany, [5]Institute of Marine Research, Fram Centre, Tromsø, Norway, [6]Christian-Albrechts University Kiel, Institute of Geosciences, Kiel, Germany, [7]National Oceanography Centre, European Way, Southampton, United Kingdom, [8]NIOZ – Royal Netherlands Institute for Sea Research, 't Horntje (Texel), Netherlands, [9]Utrecht University, Utrecht, Netherlands, [10]Scottish Association for Marine Science (SAMS), Oban, United Kingdom

Abyssal plain communities rely on the overlying water column for a settling flux of organic matter. The origin and rate of this flux as well as the controls on its fine-scale spatial distribution following seafloor settlement are largely unquantified. This is particularly true across regions where anthropogenically-induced seafloor disturbance has occurred. Here, we observed, quantified and mapped a mass deposition event of gelatinous zooplankton carcasses (pyrosomes) in July-September 2015 across one such physically disturbed region in the Peru Basin polymetallic nodule province (4150 m). Seafloor in this area was disturbed with a plough harrow in 1989 (as part of the DISCOL experiment) causing troughs in the sediment. Other parts were disturbed with an epibenthic sled (EBS) during a cruise in 2015 resulting in steep-walled, U-shaped troughs. We investigated two hypotheses: a) gelatinous food falls contribute significantly to the abyssal plain carbon pump and b) physical seafloor disturbance influences abyssal distribution of organic matter. We combined optical and bathymetric seafloor observations, to analyze pyrosome distribution on seabeds with different levels of disturbance. 2954 pyrosome colonies and associated taxa were detected in > 14,000 seafloor images. The mean regional carbon (C) deposition associated with pyrosome carcasses was significant compared to the flux of particulate organic C (182 to 1543%), and the total respired benthic C flux in the DISCOL Experimental Area (39 to 184%). EBS-disturbed seafloor tracks contained 72 times more pyrosome-associated C than an undisturbed reference site, and up to 4 times more than an area disturbed in 1989. Deposited pyrosomes collected had a higher proportion of labile fatty acids compared to the sediment. We document the temporal and spatial extent of an abyssal food fall event with unprecedented detail and show that physical seafloor disturbance results in the accumulation of detrital material. Such accumulation may reduce oxygen availability and alter benthic community

structure. Understanding both the relevance of large food falls and the fine scale topography of the seafloor, is necessary for impact assessment of technologies altering seafloor integrity (e.g. as a result of bottom-trawling or deep seabed mining) and may improve their management on a global scale.

KEYWORDS

abyssal plain, DISCOL, food fall, *Pyrosoma*, seafloor disturbance, benthopelagic coupling

Introduction

The abyssal seafloor (areas of 3000-6000 m depth) covers an estimated 75% of the global deep ocean floor surface, but *in situ* observations are still very few, with less than 1 percent explored visually by cameras and submersibles (Ramirez-Llodra et al., 2010). Abyssal plains are typically characterized by a relatively flat seafloor surface topography, predominantly composed of fine sediments (Harris et al., 2014). In oligotrophic to mesotrophic areas these plains can host high abundances of polymetallic nodules (i.e., oblate to spherical authigenic mineral concretions of typically less than 20 cm in diameter) containing a range of economically valuable metals (Hein and Koschinsky, 2014). Nodules provide hard seafloor habitat niches (Vanreusel et al., 2016; Boetius and Haeckel, 2018; Stratmann et al., 2021), increase rugosity of benthic topography on a fine scale (Simon-Lledó et al., 2019b) and alter benthic community composition and faunal density (Vanreusel et al., 2016; Simon-Lledó et al., 2020). Typically, abyssal benthic communities are highly biodiverse but with relatively low faunal densities, limited by low rates of organic matter deposition from the overlying water column (Smith et al., 2008). The majority of this organic matter originates from primary production in the photic zone. The deposition of carcasses of larger pelagic life (e.g. kelp, whales, sharks, fish, crustaceans, squid and jellyfish), also known as food falls, leads to temporarily available and highly localized patches of organic matter. Such rich depositions are set against an oligotrophic background with carcasses therefore rapidly attracting benthic and demersal megafauna scavengers (Stockton and DeLaca, 1982; Jones et al., 1998; Smith et al., 2008; Treude et al., 2009; Bernardino et al., 2010; Higgs et al., 2014). Observations of food falls on abyssal plains are rare, and their contribution to local carbon fluxes remains unquantified for many regions.

Understanding abyssal carbon fluxes is essential for evaluating the ocean's role in marine C sequestration, nutrient remineralization and biodiversity (Thurber et al., 2014), i.e. all major ecosystem services of the deep sea. Regionally, C budgets may be imbalanced where the flux of particulate organic matter measured in sediment traps is not sufficient to explain biomass and respiration rates of seafloor communities (Burd et al., 2010). This suggests that there are additional sources of C reaching the seafloor. Episodic deposition of carcasses may help to explain and partly counterbalance these C budget deficits (Smith et al., 2018), given that this flux is wholly missed by sediment-trap sampling. Gelatinous zooplankton are a prominent group in pelagic communities, fulfilling pivotal roles as both predator and prey (Robison, 2004; Lucas et al., 2014; Choy et al., 2017; Luo et al., 2020), and are therefore vectors for the transport of carbon (C) and nitrogen (N) through marine food webs. The C and N contained in the carcasses of dead gelatinous zooplankton falling to the deep seafloor is made available to benthic communities, establishing a connection between benthic and pelagic food webs (Sweetman et al., 2014; Luo et al., 2020). The available quantifications suggest significant local contributions to the C and N flux by jellyfish and pelagic tunicates (Robison et al., 2005; Lebrato and Jones, 2009; Smith Jr. et al., 2014; Sweetman and Chapman, 2015). Recent modelling and meta-analysis efforts show a global relevance of jelly falls in carbon flux (Lebrato et al., 2019) in particular in the context of warming oceans and finfish overexploitation. Carcass deposition events may also provide 'essential' fatty acids to the deep-seabed environment. Fatty acids are both principle components of lipids and an energy source and a building component of cell membranes (Burdge and Calder, 2014) as well as playing a role in signal transduction and gene expression (Burdge and Calder, 2014). Since some essential fatty acids can only be synthesized by algae or plants (with some exceptions (Pond et al., 1997; Pond et al., 2002)), they are trophic markers that are transferred conservatively from lower trophic levels (i.e., primary producers, primary consumers) to higher trophic levels and may provide indications of diets (Dalsgaard et al., 2003). Such information about diets is often unknown for abyssal fauna. Owing to a lack of observational and biochemical data, coupled with limited geographical coverage, the significance, biogeochemical contribution and fine scale distribution of gelatinous carcass deposition events in the abyssal deep sea remains uncertain. Here we quantified the deposition of pyrosome carcasses on the seafloor and analyzed their biochemical composition to test the hypothesis that jelly falls contribute significantly to local carbon budgets on the abyssal plain.

Pyrosomes are increasingly recognized as pivotal components of oceanic food webs. The pyrosome species we observed here is likely *Pyrosoma atlantica*, a species that is very common in the Atlantic, Pacific and Indian Ocean (van Soest, 1981), and recently expanded its range into the North Pacific from its typical tropical and subtropical habitats (Kuo et al., 2015; Sutherland et al., 2018; Cornwall, 2019; Décima et al., 2019; Henschke et al., 2019). Its populations may locally reach exceptionally high numbers (200,000

kg WM km^{-3} (Brodeur et al., 2019)), clogging fishing nets and waste water treatment plants. Pronounced ecological impacts of pyrosome blooms include reductions in crustacean zooplankton (Sakuma et al., 2016), and high grazing impact. In one grazing event 22% of the phytoplankton stock in the Northern California Current offshore Oregon (USA) were consumed by pyrosomes (O'Loughlin et al., 2020). Pyrosomes occur in high densities in midwater, forming a biological substrate for pelagic crustaceans. They migrate on a daily basis from mesopelagic depths at night to the surface, to benefit from the increased productivity of sunlit waters. Pyrosome food falls may contribute significantly to local carbon fluxes in the Atlantic and Pacific and attract a diversity of megafaunal scavengers. Quantifications of the biogeochemical contribution of pyrosome food falls on the abyssal plain are absent at the time of writing.

A pressing question in deep-sea ecology is how seafloor disturbance may alter food distribution. Abyssal food availability is spatially variable. The spatial heterogeneity of food availability appears to be controlled by local hydrodynamic regimes, often affected by topography across fine (centimeters to meters) (Snelgrove et al., 1994) and broad landscape scales (Durden et al., 2015; Simon-Lledó et al., 2018). Temporal patterns include clear seasonal and inter-annual variation in C flux (Smith and Kaufmann, 1999; Durden et al., 2020). Long-term variations with associated impacts on the benthos also result from climatic variations (Smith et al., 2013; Soltwedel et al., 2016; Sweetman et al., 2017). This heterogeneity can structure deep-sea communities at various spatial and temporal scales and hence is relevant to local biodiversity (Grassle and Morse-Porteous, 1987), community structure, and affect functional processes, such as bioturbation and C distribution, cycling and remineralisation (Thurber et al., 2014). The combined interaction of abyssal benthic fauna and microbes results in a higher proportion of C stored in the seafloor sediments, when compared to nutrients such as N and P, of which a greater relative proportion is re-mineralized and released back into the ocean (Van Cappellen, 2003). Disturbing the biologically active layer of the deep-sea sediment (e.g. via anthropogenic activities) is therefore expected to alter the processing of C within sediments (Vonnahme et al., 2020), but may cause other impacts on seabed ecosystems as well. For example, the increased roughness which can result from direct physical disturbance of the seafloor can also influence the deposition of organic matter by altering the hydrodynamical and mechanical processes governing the spatial distribution of organic matter deposition, as shown for coastal systems in laboratory experiments (Yager et al., 1993) and in the field (Cacchione et al., 1978; Lebrato and Jones, 2009). Today, little information is available on the interaction between seafloor physical disturbance and organic matter deposition in the deep sea (König et al., 2001), even though large areas of seafloor have already been disturbed by deep-sea fisheries (Gage et al., 2005; Sala et al., 2021). It is likely that physical impacts on seafloor integrity influence not only the release of inorganic C (Sala et al., 2021), but also the spatial distribution of organic matter deposition in the deep sea. This hypothesis has not been tested, owing to the stochastic, thus hard to predict, nature of zooplankton blooms and other large-scale organic matter deposition events in the deep-sea.

One of the most comprehensive experiments aimed at assessing the impacts of deep-sea sediment disturbance to date, the so-called 'Disturbance and Recolonization Experiment' (DISCOL), commenced in 1989 in an area of abundant polymetallic nodules (>4000 m depth) in the Peru Basin, southeast Pacific (Thiel, 1991; Thiel et al., 2001). At that time, the seafloor was physically disturbed by dragging a plough-harrow almost 78 times across a nodule-covered area of 10.8 km^2, ploughing most of the nodules under the overturned sediment surface (Thiel and Schriever, 1989; Thiel et al., 2001). The effects of seafloor disturbance on the deposition of organic matter were studied here using the results from a research cruise that returned to the DISCOL site 26 years after the initial disturbance as part of the European project MiningImpact (Greinert, 2015). The plough tracks from 1989 were still clearly visible in 2015 (Gausepohl et al., 2020), when additional trawl tracks were created with an epibenthic sled (EBS) to collect epifauna. Using an array of observational tools, we quantified zooplankton food falls to determine if gelatinous carcasses contribute significantly to the local carbon pump of the abyssal plain of the Peru Basin. We also investigated the effect of physical impacts on seafloor integrity, as induced by ploughing and trawling disturbance, on the local C deposition of sinking food fall material within the deep sea.

Methods

Study site

The DISCOL area (07° 04.40 ' S/088° 27.60 ' W) lies in the Peru Basin (Southeast Pacific) between 3,850 m and 4,250 m water depth (Figure 1). Towards the south and east extent of the area, the morphology of the area is gentler, consisting of large basins descending from 4,150 m water depth at the DISCOL experimental area (DEA) down to 4,250 m water depth. The DEA itself covers an area of 3.7 km diameter, the centre of which is situated in a 25 m deep N-S striking valley of 1.4 km width (Figure 2).

Sediment disturbance creation

During the DISCOL experiment in 1989, an 8-m wide plough-harrow was ploughed 78 times across the circular DISCOL experimental area (DEA; diameter: 3.7 km) creating plough tracks (Figure 2). These tracks altered seafloor integrity by creating troughs (approximately 20 cm in 2015) (Paul et al., 2019), depressions, piles and ridges in the sediments (Vonnahme et al., 2020) (Figure S1). By disturbing the biologically active layer, microbial and benthic faunal communities were altered and with that the biogeochemical properties of the seafloor (Haeckel et al., 2001; Vonnahme et al., 2020).

During *RV Sonne* cruise SO242 leg 1 (28 July 2015 – 25 August 2015), a fresh seafloor disturbance were created with an epibenthic sled (Greinert, 2015) (EBS) towed across previously unploughed, nodule-abundant seafloor, starting with the first EBS track on 5 August 2015 (#081-EBS-3) and the second EBS track on 13-14

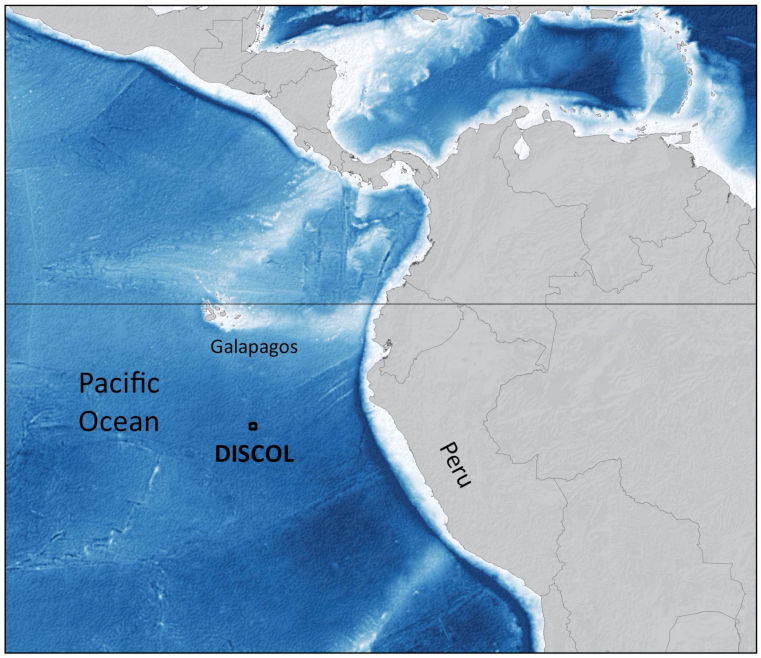

FIGURE 1
DISCOL Experimental area in the Peru Basin. Geographic location of the DISCOL area.

August 2015 (#085-EBS-4) (Figure 2). The purpose of conducting these new EBS deployments was to create a disturbance with freshly exposed deeper suboxic and more compacted sediment strata for infauna and biogeochemical process impact analyses. The EBS disturbance differed somewhat in nature from the initial plough-harrow disturbance methodology employed in 1989. The EBS pushes material to the side, resulting in the formation of a steep, a few 10s of cm deep, U-shaped through approximately 2 m wide, in which polymetallic nodules are completely removed. Compared to the 1989 plough tracks, the EBS disturbance exposed more compacted sediment from below the bioturbated layer, which have a more heterogeneous character. The recent EBS trawling tracks also resulted in piles of overturned sediment blocks smothering seafloor surface sediments, with deeper, potentially less oxygenated and nutrient-abundant sediments displaced onto the adjacent seafloor sediments. The disturbance of the EBS resulted

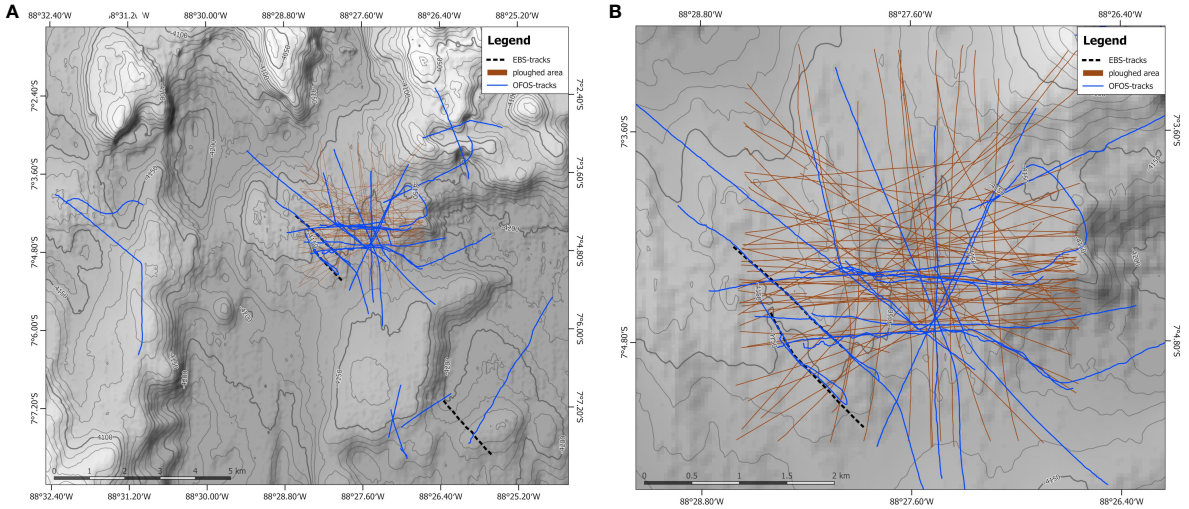

FIGURE 2
Bathymetric maps of the survey area. **(A)** The complete seafloor area that was surveyed during SO242. **(B)** the DISCOL Experimental Area. The plough tracks from 1989 are indicated in brown lines, and the EBS tracks from 2015 are in a dashed black line, the Ocean Floor Observations System (OFOS) tracks are in blue. Bathymetric data were acquired during cruise SO242 and published by Gausepohl et al. (2019; https://doi.org/10.1594/PANGAEA.905579).

in 15 – 20 cm deep track marks with steep sides (Vonnahme et al., 2020), contrasting with the older plough harrow tracks, that were similar in depth but had smoother and more gently sloping sides (Figure S1).

Seafloor imagery

During SO242 leg 1, 6 video transects (covering 3.6 km) were conducted between 3 August and 23 August 2015, with a custom-built Ocean Floor Observation System (OFOS) (Greinert, 2015). During *RV Sonne* cruise SO242 leg 2, OFOS collected more than 14,000 seafloor images during 16 transects from 31 August to 25 September 2015 each of which covered between 462 and 7,365 m^2 of seafloor area and collected between 88 and 1,403 images per transect (Table S1). OFOS was towed at an altitude of 1.7 m above the seafloor and used a 23 megapixel downward-facing still camera (iSiTEC, Canon EOS 5D Mark III) to take images every 15 s, each of which also captured the laser points projected by a tri-laser (50 cm spacing) sizing device (iSiTEC, custom built). Ship speed was maintained at 0.1–0.2 m s^{-1} (Boetius, 2015). After imagery collection, the seafloor within each image was characterized as representing one of four contrasting categories of seafloor type, following earlier classification (Bluhm et al., 1995), and a corrected version (Bluhm, 2001). These categories were: 1) Disturbed Areas (inside plough mark in DEA), 2) Undisturbed Areas (outside plough mark in DEA, but showing various levels of re-sedimentation of sediment plumes created by the ploughing), 3) Reference Areas (outside DEA, not affected by ploughing) with polymetallic nodules, and 4) Reference Areas without polymetallic nodules. A fifth category of seafloor was added to represent images of the seafloor disturbed by the EBS trawl; 5) EBS disturbed seafloor. However, sidescan sonar imaging conducted during the cruise revealed some inconsistencies in Bluhm's category 4, as nodule patches were detected in the seabed area representing this category (Reference East); the only relatively large nodule-free areas (i.e. low backscatter) across the study area were found within the DEA[43]. For the current study, the focus was on the accumulation of pyrosomes across physically undisturbed and disturbed areas of seafloor. With this in mind, we defined three seafloor categories: "Undisturbed" includes the categories with no physical disturbance 2 to 4 (see above), "plough-disturbed" corresponds to category 1 above, and "EBS disturbed" is category 5 above.

All seafloor images were inspected, the number of pyrosome carcasses quantified and the seafloor category noted. In cases where more than one habitat category was present in an image, the image was identified as belonging to the most spatially dominant category. Pyrosome densities were calculated by dividing the number of pyrosomes by the area surveyed. Image scaling was conducted by measuring the spacing of the laser points in a subset of 3,663 images using the PAPARA(ZZ)I software application (Marcon and Purser, 2017). The image area of all remaining images was calculated from the camera altitude (distance to seafloor) using a second-order polynomial regression of the laser-based measurements. The average seafloor image area was 5 m^2 (interquartile range 4.45 – 6.25 m^2). To determine the average dimensions of the pyrosome carcasses observed on the seafloor, 20 pyrosome colonies were measured on OFOS images collected on each of three different days (onset of pyrosome carcass deposition: 10 August 2015; maximum carcass deposition: 16 September 2015; decline of carcass deposition: 25 September 2015) using the PAPARA(ZZ)I software application (Marcon and Purser, 2017). A one-way ANOVA was conducted using the SPSS 17.0 software application to determine whether pyrosome lengths differed significantly by date of observation.

Additionally, pyrosome colonies were opportunistically imaged when observed on the seafloor during seafloor activities conducted by the remotely operated vehicle ROV KIEL 6000 (GEOMAR, Kiel, Germany). Associations between the carcasses and other organisms, such as scavengers, were also recorded. High-resolution photographs (24 Megapixel) of such pyrosome colony associations were taken by the SubC-Imaging 1 Alpha Cam, which was mounted on the lower pan & tilt unit of the ROV KIEL 6000.

Water column imagery

ROV KIEL 6000 was deployed 22 times during SO242/2 to a maximum depth of 4,160 m. The ROV was equipped with two colour zoom cameras (Kongsberg OE14-366, standard definition (SD), PAL, resolution 470 TV lines, recorded with 720x756 pixel, Mpeg encoded), which recorded footage continuously throughout the entire ROV dives including the water column during downcast and upcast. The cameras were mounted on a lower and an upper pan & tilt unit, respectively. During downcast and upcast, both SD cameras were usually pointed forward and zoomed out.

After an initial inspection of the SD video footage, the depth intervals for analysis per dive were defined as 300 to 450 m on downcast and 450 m to the surface on upcast (depth sensor data are shown in the image overlay). Videos of both SD cameras were inspected for all stations except one when the depth could not be determined due to malfunction of sensor. Numbers of pyrosome colonies present in the water column were categorized as 1) possible, 2) occasional (1 – 5 ind.), 3) numerous (6 – 22 ind.) and 4) many (50+ ind.). For graphical illustration, the higher density category of both downcast and upcast was chosen for each dive.

Pyrosome carcass collections and processing

Pyrosome carcasses were collected (n = 3) from the seafloor using the manipulator arm of the ROV KIEL 6000, stored in its "biobox", and recovered to the vessel where they were measured, weighed and stored frozen at -20°C. Pyrosome biomass (g org. C $pyrosome^{-1}$) was determined by total length (TL)-wet mass (WM) relationships and subsequent conversion to dry mass (DM), organic carbon content (orgCC), and total nitrogen content (TNC) using conversion factors.

WM (g WM $pyrosome^{-1}$) of pyrosomes was calculated following the equation (Miller et al., 2019):

$$WM_{pyrosome} = 3.6 \times 10^{-4} \times TL_{pyrosome}^{2.32}$$

with the mean pyrosome length (from photographs) from 2015 (133 ± 5 mm). This resulted in a WM of 30.5 g WM pyrosome^{-1}.

DM (% WM) was determined from three collected pyrosomes. At the shore-based laboratory facilities of NIOZ-Yerseke (the Netherlands), the frozen pyrosomes were weighted on a precision balance, freeze-dried, and weighted again to determine DM. Subsequently, the individual freeze-dried pyrosomes were ground to fine powder with mortar and pestle and organic C and N content as well as their stable isotope signature $\delta^{13}C$ and $\delta^{15}N$ in ~10 mg pyrosome tissue were measured with a Thermo Flash EA 1112 elemental analyzer (EA; Thermo Fisher Scientific, USA). Results of the stable isotope analysis were presented in standard δ notation (‰) as:

$$\delta X = \frac{(R_{sample} - R_{standard})}{R_{standard} \times 1000}$$

where X corresponds to ^{13}C and ^{15}N, respectively, and R is the ratio of $^{13}C/^{12}C$ and $^{15}N/^{14}N$, respectively.

Pyrosome biomass (g C pyrosome^{-1}, g TN pyrosome^{-1}) was calculated as:

$$orgCC_{pyrosome} = WM_{pyrosome} \times DM_{pyrosome}conversion \times C_{pyrosome}conversion$$

with $DM_{pyrosome}$ conversion = 0.047 and $C_{pyrosome}$ conversion = 0.085, because DM of the three pyrosomes was 4.70 ± 0.08% WM and orgCC of the pyrosomes was 8.51 ± 1.45% DM.

$$TNC_{pyrosome} = WM_{pyrosome} \times DM_{pyrosome}conversion \times TN_{pyrosome}conversion$$

with $TN_{pyrosome}$ conversion = 0.0199, because the TNC of the freeze-dried pyrosomes was 1.99 ± 0.38% DM.

Biochemical analysis of pyrosome tissue and deep-sea sediment

Total fatty acids (tFA) were extracted from ~110 – 250 mg freeze-dried and homogenized pyrosome tissue powder with a modified Bligh and Dyer extraction method (Bligh and Dyer, 1959; Boschker, 2008): The pyrosome powder was mixed with 6 ml MilliQ-water, 15 ml ultra-pure methanol (HPLC grade, 99.8%), and 7.5 ml ultra-pure chloroform (HPLC grade, 99.5%) in pre-cleaned test tubes. Prior to use, these tubes and all other glass ware were washed in the dishwasher and subsequently rinsed with ultrapure *n*-hexane (HPLC grade) and methanol. After shaking for 2 h, 7.5 ml chloroform were added, the tubes were shaken again, and 7.5 ml MilliQ-water were added. The tubes were stored at -21°C over night to let the solvent layers separate. The lower layer contained the chloroform extract that was transferred to pre-weighed test tubes. The weight of this chlorofom extract was determined before it was evaporated to complete dryness. About 0.5 ml chloroform was added to the test tube and evaporated again. For the derivatisation of tFAs to fatty acid methyl esters (FAMEs), 1 ml methanol-toluene mix (1:1 volume/volume), 20 µl of a first internal standard (1 mg 19:0 FAME mL^{-1}), and 1 ml 0.2 M metanolic NaOH (0.58 g Na in 100 g methanol) were added to the test tube containing the tFA extract. After 15 min of incubation at 37°C, 2 ml *n*-hexane, 0.3 ml 1 M acetic acid, and 2 ml MilliQ-water were added and the solution was mixed very well. After the layers had separated, the (upper) *n*-hexane layer was transferred to new test tubes, 2 ml *n*-hexane were added to the old test tubes containing the acetic acid-MilliQ-water solution, and the step was repeated. The *n*-hexane layer was transferred to the same new tubes and 20 µl of a second internal standard (1 mg 12:0 FAME mL^{-1}) were added. The *n*-hexane was evaporated to complete dryness and the FAMEs were transferred in 200 µl *n*-hexane to measuring vials. All FAMEs were separated on a BPX70 column (50 m length, 0.32 mm inner diameter, 0.25 µm film thickness; SGE Analytical Science) with a HP 61530 gas chromatograph (Hewlet Packard/ Agilent, USA). Their concentrations (µg C g DM pyrosome^{-1}) and $\delta^{13}C$ values (‰) were measured on a Finnigan Delta Plus IRMS (Thermo Fisher Scientific, USA) that was coupled with the gas chromatograph via a combustion GC-c-III interface (Thermo Fisher Scientific, USA). Peaks of the FAME chromatogram were identified based on the equivalent chain length (ECL) and the peak area was calculated using the two internal standards (12:0 and 19:0) for area correction.

Total NLFAs and PLFAs in pyrosome tissue were extracted from similar amounts of freeze-dried, homogenized pyrosome powder as described above. After the extraction, 0.5 ml chloroform was added to the test tube containing the total lipid extract. This extract was fractionated into different lipid classes over a silicic acid (Merck Kieselgel 60; activated by heating to 120°C for min. 2 h) column by eluting with 7 ml chloroform, 7 ml acetone, and 15 ml methanol. The aceton fraction was discarded, but the chloroform fraction containing the NLFAs and the methanol fraction, in which the PLFAs were dissolved, were collected in separate test tubes and evaporated to dryness. NLFAs and PLFAs were derivatized to FAMEs by mild alkaline transmethylation as described for tFA above, separated on the same BPX70 column and measured on the same GC-c-IRMS.

Concentrations of essential PLFAs in pyrosomes deposited at a specific seafloor area (c(essential $PLFA_{pyrosome,\ spatial}$), mg C m^{-2}) were calculated as follows:

$$c(essential\ \ PLFA_{pyrosome,\ spatial}) = density_{pyrosome} \times DM_{pyrosome} \times PLFA\ \ content_{pyrosome}$$

PLFAs were also measured for deep-sea sediment. Sediment samples were extracted from 0 – 2 cm and 2 – 5 cm sediment layers as stated in (Stratmann et al., 2018a). Briefly, PLFAs from 2.5 g freeze-dried sediment were extracted following the same protocol that was used for pyrosomes (see above). The total lipid extract was fractionated into lipid classes over the silicic acid column and the PLFAs in the chloroform fraction were derivatized to FAMEs as mentioned above. Subsequently, the FAMEs were separated on a ZB5-5MS column (60 m length, 0.32 mm diameter, 0.25 µm film thickness; Phenomenex, USA) and their concentrations and $\delta^{13}C$ values were determined by the same GC-c-IRMS that was used for tFAs- PLFA-, and NLFA-FAMEs from pyrosome tissue.

Calculation of pyrosome deposition rate

To calculate the pyrosome C and N contribution across the differing disturbed and undisturbed seafloor categories of the study region, we multiplied the above calculated pyrosome density (pyrosome m^{-2}) by the pyrosome C and N content, which was 0.12 g C $pyrosome^{-1}$ and 0.03 g N $pyrosome^{-1}$.

Calculating the deposition rate of pyrosome colonies and hence C and fatty acid flux was somewhat hampered by the temporal restrictions of our data. There were no data available beyond the cruise duration and hence we do not know the full duration of this deposition event, i.e. if the observed pyrosome bloom was a temporary event or if deposition happens throughout the year. Additionally, the removal rates were not rates of pyrosome removal, but of *Phacellaphora camtschatica* that is not scavenged by fish (Sweetman, personal observation). Hence, the removal rate in the DISCOL area could be higher than calculated here. On the other hand, experimental food falls of pyrosomes in Monterey Bay were still largely untouched on the seafloor after 24 hours (Hoving, personal observation).

Statistical analysis of seafloor observations

Our main variable of interest was the calculated pyrosome density, labeled Pyrosome *concentration* (Table S1), as measured by the pyrosomes encountered per square meter of the area imaged. Our unit of analysis was the density per day, $(C_{i,t})$ t =1, …, 26, by area classification, i =, U,E,P, where U represents undisturbed seafloor, E the EBS disturbed seafloor, and P the plough-disturbed seafloor. Note that although our unit of analysis was at the date/classification level, each cross-sectional unit represented a unique area imaged.

In order to test our hypothesis that seafloor classification had an impact on the observed pyrosome density, we required two modifications of the raw data. The first modification was motivated by theoretical considerations. If no pyrosomes were encountered, reflected by a density level equal to zero in the data, it could be considered possible that either pyrosomes were never present in the first place, or that pyrosomes were at some point present but the seafloor was highly unfit to maintain the pyrosome presence. As both possibilities are *observationally* equivalent, we regarded it as inappropriate to include these observations in testing our main hypothesis. Therefore, we excluded the days when we observed no pyrosomes from statistical analysis. The second modification was a simple transformation of the variable of interest; the distribution in density was highly skewed and of course non-negative, rendering it unlikely that residuals be normally distributed. We therefore assumed that density levels were log-normally distributed, and used the natural logarithm of the pyrosome density in our analysis accordingly.

Figure 3 visualizes the modified data over time, by seafloor classification. Two observations stand out in this figure. First, our panel data set was rather unbalanced, both over time and in cross-

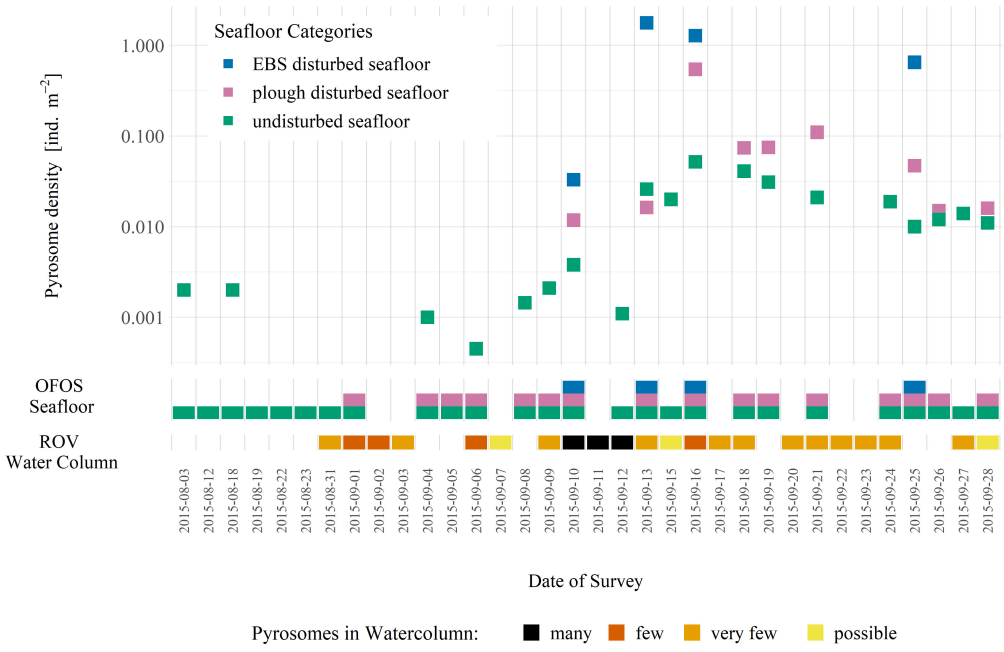

FIGURE 3
Temporal change of observed pyrosomes in the DISCOL Experimental Area in 2015. Seafloor observations with Ocean Floor Observations System (OFOS) allowed quantification of pyrosome densities (y-axis) over time (x-axis). The blue, pink and green symbols on the primary x-axis (OFOS Seafloor) indicate OFOS surveys in EBS, plough-disturbed and undisturbed seafloor, respectively. On all dives with the remotely operated vehicle (ROV), pyrosomes in the water column were estimated and illustrated on the secondary x-axis (ROV Water Column). Degrees of presence include possible (shapes in distance that are not identified as pyrosomes with confidence), occasional (1-5), numerous (6-22) and many (>50) is indicated by colours. Absence of a square on the x-axis under "OFOS Seafloor" and "ROV Water Column" equals no data collection. Absence of a y-value on a day with surveys means no pyrosomes were observed. Note the logarithmic scale on the y-axis.

section, and second, the overall variation over time (*within variation* = 1.88) was large compared to the variation between seafloor classification (*between variation* = 1.14). Moreover, a clear dynamic pattern was visible in the data, directly related to the pyrosome bloom.

To assess the differences in density per seafloor classification we used a *time fixed effects* regression, which accounted for differences in overall average levels of density over time, for all seafloor types. Though there may be more efficient and/or powerful tests to account for dynamic patterns, we approached the bloom effects in a statistically robust manner instead of trying to parametrically model the dynamic pattern. The only implicit assumption we made by doing so was that the temporal pattern affected all seafloor types in a homogenous way. We acknowledge that there may be particular deviations for each unique imaged area, but these were reflected by the residuals, and we assumed that there was no particular bias in these deviations. To detect statistical differences for the seafloor classification, we ran these regressions with an EBS dummy variable and a Plough-disturbed dummy variable, capturing differences in log density relative to undisturbed seafloors.

To justify our assumption of log-normality and the associated statistical inference, we conducted a test for normality on the residuals and provide a normal-quantile plot (Figure S3). Based on the separate skewness and kurtosis tests, as well as a joint test on both skewness and kurtosis, we cannot reject that the residuals are normally distributed. Moreover, the quantile plot (Figure S3) shows some slight deviation in the tails, yet nothing too severe as to qualitatively affect our tests.

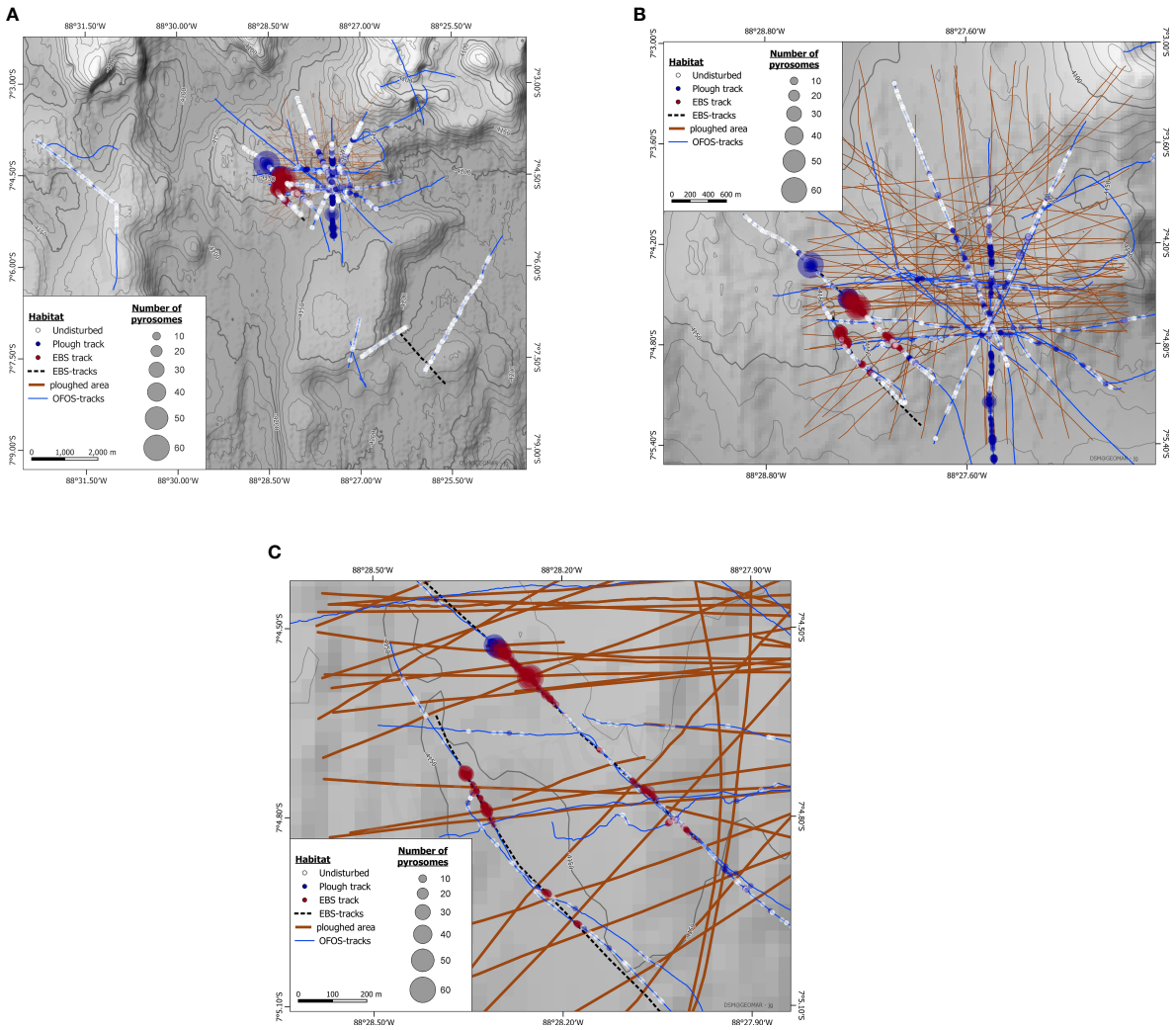

FIGURE 4
Pyrosome deposition in relation to seafloor type. **(A)** Overview of pyrosome deposition in the complete area surveyed during SO242, **(B)** Pyrosome deposition in the DISCOL Experimental Area. **(C)** Detail of **(B)** showing the southwest DISCOL region that was disturbed with epibenthic sled (EBS) and where most pyrosomes were observed. The circles indicate the presence of pyrosome carcasses observed along a track with the Ocean Floor Observation System (blue), and the colour of the circles indicate the seafloor type (undisturbed, plough track, EBS) where the pyrosomes were observed. The size of the circles depicts the number of pyrosomes in an image, showing that more pyrosomes were observed in the EBS and plough tracks than on the undisturbed seafloor. Images were collected throughout all transects with a spacing of several meters. Where no circles are placed over a survey track, no pyrosomes were observed.

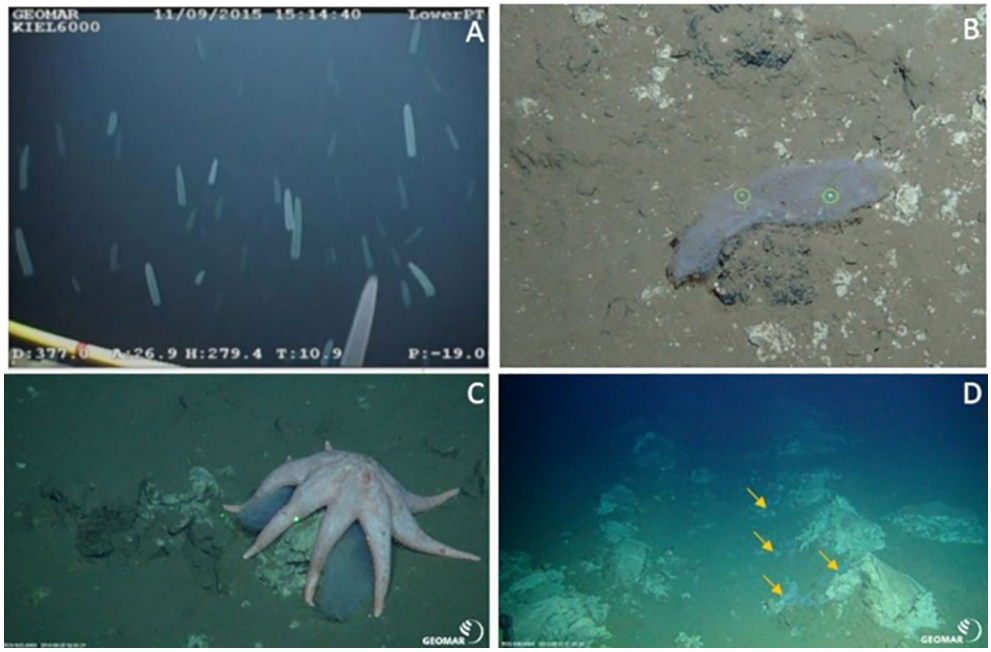

FIGURE 5
In situ observations of pyrosomes by ROV KIEL 6000 in the water column and on the seafloor. **(A)** Pyrosomes in the water column during ROV descent in the morning of 11.09.2015. **(B)** A pyrosome on the seafloor next to a polymetallic nodule at 4,150 m in the DISCOL area illustrating that seafloor rugosity can stop pyrosomes from travelling with currents. **(C)** A seastar presumably feeding on pyrosomes in the EBS track. **(D)** Pyrosomes in the EBS track, indicated by yellow arrows, showing accumulation of pyrosomes on one side of the EBS track (Images: ROV Team GEOMAR). (Laser points on **B, C** are 6.3 cm apart, and indicated by green circles).

Results

Temporal change in abundance of pyrosomes

Pyrosomes were observed and quantified on the seafloor by the OFOS (Figures 3, 4) and documented in both the water column and seafloor by the ROV (Figures 3, 5). The first water column observations were made on ascent on 31 August 2015, followed by a peak in water column pyrosome counts in observations between 10 and 12 September 2015 when many (> 50) pyrosomes were observed in the water column during ROV descents and ascents (Figure 3). Subsequently, numerous (6 – 22) or occasional (1 – 5) pyrosomes were seen within the water column between 17 September 2015 and the end of the cruise station work on 28 September 2015. The ROV was only on board the ship on cruise leg 2.

Few dead pyrosomes were observed during SO242/1 on the seafloor. AUV surveys documented ~5 dead pyrosomes in 100,000 m^2 of seabed surveyed across the DISCOL site (Simon-Lledó personal observation) and OFOS observed 2 pyrosomes during 6 transects across the undisturbed area (Table S2). During SO242/2, pyrosomes were observed on the seafloor on 3 August 2015 during an OFOS survey across the undisturbed areas (Figures 3, 4; Table S1). During the following 12 OFOS surveys in undisturbed areas, pyrosomes were occasionally visible (max. density 0.002 pyrosomes m^{-2} on 9 September 2015) and only during five surveys. At these times, none were observed during five OFOS surveys in the DEA. Pyrosomes were, however, increasingly present on OFOS images taken on transects on and after 10 September 2015, during which pyrosomes were observed in all three areas (plough tracks, EBS tracks and undisturbed) (Figure 3).

On 13 September 2015 the overall highest pyrosome seafloor density was recorded (in the tracks of the EBS; 1.77 pyrosomes m^{-2}) (Figures 3, 4: Table S1). Densities of pyrosomes across both the undisturbed and plough-disturbed areas reached maxima (0.052 and 0.54 pyrosomes m^{-2}, respectively) on 16 September 2015, but were lower than in the freshly trawled EBS tracks on the same day (1.28 pyrosomes m^{-2}) (Figure 3; Table S1). The peak abundance observed on 16 September 2015 was followed by a gradual decrease in pyrosome densities on the seafloor across all seafloor categories, with the declining trend in abundances sustained until the end of the survey period. On 25 September, the last day with surveys conducted in all habitat areas, pyrosomes showed low densities on the undisturbed seafloor (0.01 pyrosomes m^{-2}), higher densities in the plough-disturbed area (0.047 pyrosomes m^{-2}) and highest densities in the EBS track (0.65 pyrosomes m^{-2}) (Table S1). Repeated observations in the same region confirmed a similar pattern in pyrosome densities.

Pyrosome accumulation in disturbed seafloor areas

Average densities in the undisturbed areas were 0.01 ± 0.01 pyrosomes m^{-2} (with and without including zero values), and in the

plough-disturbed areas this was 0.06 ± 0.13 (including zero values) and 0.1 ± 0.17 (excluding zero values) in the plough-disturbed areas. In the EBS areas the average density was 1.01 ± 0.64 (no zero values). Fixed time effects regression confirmed that there were significant differences in pyrosome density between seafloor classifications (Table S2). Overall, the pyrosome densities in both disturbed areas were significantly higher than in the undisturbed seafloor classification areas (point estimate for EBS dummy variable = 3.88, significance = 1%, *t*-stat = 8.65; point estimate for plough-disturbed dummy variable = 0.97, significance = 5%, *t*-stat = 3.00) (Table S2).

Pyrosomes appeared to accumulate against vertical or sloped edges of the flanks of track marks from the plough and the EBS (Figure 5; Figure S1). Individual pyrosomes were additionally observed in association with polymetallic nodules (Figure 5), or the stalks of sponges or crinoids.

Biochemical composition of pyrosomes

During the onset of the pyrosome carcass bloom on 10 September 2015, pyrosomes had a mean total length (TL) of 13.3 ± 4.1 cm (n = 20) and on 16 September 2015, the day the maximum density of carcasses was observed on the seafloor, TL was 13.6 ± 3.7 cm (n = 20). During the decline of pyrosome carcass density on the seafloor on 25 September 2015, the mean TL was 13.0 ± 7.1 cm length (n = 20). The overall mean pyrosome TL was 13.3 ± 0.5 cm (n = 60) and did not differ significantly between the different dates of observations (one-way ANOVA test, $F(2,57) = 0.056$, $p>0.05$).

Carbon content of pyrosomes was 8.51 ± 1.77% C dry mass (DM) pyrosome^{-1} (n = 3) and their $\delta^{13}C$ value was -22.0 ± 0.08‰ (n = 3). Pyrosomes contained 1.99 ± 0.38% nitrogen (N) DM pyrosome^{-1} (n = 3), had a $\delta^{15}N$ value of 2.59 ± 0.37‰ (n = 3) and a C/N-ratio of 4.86 ± 0.34 (n = 3). Furthermore, they included 689 ± 109 µg total fatty acids (tFA)-C g DM pyrosome^{-1}, of which 86.1 ± 25.2% consisted of PLFAs and 11.9 ± 4.57% of NLFAs (Table 1). Highly unsaturated fatty acids (HUFAs; i.e., fatty acids with ≥4 double bonds) contributed with 47% most to tFAs, followed by saturated fatty acids (SFAs) with 28%, and PUFAs (i.e., fatty acids with ≥2 double bonds) (15%) (Table 1). Pyrosome PLFAs were similarly dominated by HUFAs and SFAs, whereas NLFAs contained 28% SUFAs, 22% HUFAs, and 21% PUFAs. About 64%, 92%, and 75% of these PUFAs of tFAs, PLFAs, and NLFAS, respectively, were 'essential fatty acids'(Dalsgaard et al., 2003) and ALA (co-eluted with oleic acid, 18:1ω9) (Table 1). Other abundant fatty acids in pyrosomes were adrenic acid (22:4ω6) (tFA: 20%, PLFA: 21%) and palmitic acid (16:0) (NLFA: 8%) (Tables 1, 2).

In addition to the dominant PLFAs, pyrosomes contained PLFAs that have been identified as trophic markers for specific food sources (Table 2): Pyrosomes had low concentrations of gondoic acid (20:1ω9; co-eluted with 20:3ω3) and 22:1ω11 (together 0.3% of total PLFAs, Table 2), which are markers for calanoid copepods [Table 2, (Dalsgaard et al., 2003)]. They also contained low concentrations of stearidonic acid (18:4ω3), 20:4ω3, and eicosapentaenoic acid (EPA, 20:5ω3) (together 12% of total PLFAs; Table 2) that are markers for brown macroalgae (Phaeophyta), and low concentrations of the markers for Prymnesiophyceae, i.e., oleic acid, moroctic acid (18:4ω3), and

TABLE 1 Biochemical composition of pyrosomes (n = 3) and sediment collected in the DISCOL area in 2015.

	Total fatty acid in pyrosomes	PLFA in pyrosomes	NLFA in pyrosomes	PLFA in sediment	
				0–2 cm	2–5 cm
Total concentration (µg C g DM pyrosome^{-1}, µg C g DM sediment^{-1})	689 ± 109	497 ± 146	68.9 ± 26.3	2.01 ± 0.85	2.15 ± 0.43
Contribution of SFA (%)	27.8 ± 2.22	28.5 ± 3.71	27.6 ± 1.46	36.1 ± 2.82	52.1 ± 15.1
Contribution of MUFA (%)	8.54 ± 2.42	8.47 ± 0.16	19.7 ± 3.54	41.9 ± 2.08	31.3 ± 8.52
Contribution of PUFA (%)	14.9 ± 1.35	15.4 ± 1.15	20.5 ± 4.68	11.0 ± 0.52	8.25 ± 2.94
Contribution of HUFA (%)	46.6 ± 2.67	46.3 ± 3.94	22.2 ± 3.36	1.98 ± 1.45	0.60 ± 0.84
Contribution of LCFA (%)	0.95 ± 1.04	1.03 ± 1.46	8.45 ± 7.74	0.30 ± 0.43	0.92 ± 1.31
Contribution of cyclopropyl fatty acids (%)	0.07 ± 0.08	0.01 ± 0.02	0.56 ± 0.79	2.02 ± 0.40	1.19 ± 0.90
Contribution of 10-methyl fatty acids (%)	1.10 ± 1.26	0.15 ± 0.11	1.01 ± 1.43	6.78 ± 0.84	5.66 ± 2.33
Contribution of hydroxy fatty acids (%)	0.06 ± 0.04	0.02 ± 0.03	0.00 ± 0.00	not detected	not detected
Total concentration of essential fatty acids 18:2ω6 (linoleic acid) and 18:3ω3 (α-linolenic acid ; co-eluted with 18:1ω9, oleic acid) in pyrosome carcass (*n* = 3) and sediment samples (*n* = 3)	63.6 ± 33.3 µg C g DM pyrosome^{-1}	68.4 ± 12.0 µg C g DM pyrosome^{-1} (equivalent to: 0.10 ± 0.06 mg C m^{-2} in EBS track; 0.006 ± 0.013 mg C m^{-2} in plough track; 0.001 ± 0.001 mg C m^{-2} at undisturbed seafloor)	9.28 ± 1.54 µg C g DM pyrosome^{-1}	0.12 ± 0.04 µg C/g DM sediment (equivalent to: 0.48 ± 0.05 mg C m^{-2})	0.11 ± 4.23×10^{-3} µg C/g DM sediment (equivalent to: 0.43 ± 0.11 mg C m^{-2})

DM, dry mass; HUFA, highly unsaturated fatty acids (fatty acids with ≥4 double bonds); LCFA, long-chain fatty acids (fatty acids with ≥24 C atoms); MUFA, monounsaturated fatty acids (fatty acids with one double bond); NLFA, neutral lipid-derived fatty acid; PLFA, phospholipid-derived fatty acid; PUFA, polyunsaturated fatty acids (fatty acids with ≥2 double bonds); SFA, saturated fatty acids.

TABLE 2 Sources of fatty acids in the pyrosomes from the DISCOL area (Peru Basin).

Fatty acid	Origin	Ref.
20:1ω9, 22:1ω11	Calanoid copepods	(Falk-Petersen et al., 1987; Dalsgaard et al., 2003)
16:3ω3, 16:3ω4, 16:4ω3, 18:1ω7, 18:2ω6, 18:3ω3, 18:3ω6, 18:4ω3, 20:4ω3	Chlorophyta (green macroalgae)	(Léveillé et al., 1997; Graeve et al., 2002; Kelly and Scheibling, 2012; Gaillard et al., 2017)
14:0, 18:1ω9, 18:2ω3, 18:2ω6, 18:4ω3, 20:4ω6, 20:5ω3	Phaeophyta (brown macroalgae)	(Graeve et al., 2002; Kelly and Scheibling, 2012; Gaillard et al., 2017)
18:1ω9, 18:4ω3, 22:5ω6	Prymnesiophyceae	
16:1ω7, 16:2ω4, 16:2ω7, 16:3ω4, 16:3ω6, 16:4ω1, 20:5ω3; 16:1ω7/16:0-ratio >1; 20:5ω3/22:6ω3-ratio >1	Diatoms	(Jeffries, 1970; Mayzaud et al., 1989; Skerratt et al., 1995; Léveillé et al., 1997; Perissinotto et al., 2007; Kelly and Scheibling, 2012)
16:0, 16:3ω4, 18:0, 18:2ω6, 18:3ω3, 18:4ω3, 18:5ω3, 20:5ω3, 22:6ω3; 16:1ω7/16:0-ratio <1	Dinoflagellates	(Jeffries, 1970; Mayzaud et al., 1989; Skerratt et al., 1995; Léveillé et al., 1997; Kelly and Scheibling, 2012)(Perissinotto et al., 2007)
12:0, 14:0, *i*15:0, *ai*15:0, 16:0, 16:1ω7, cy-17:0, 18:1ω7, 18:0, cy-19:0	Bacteria	(Parkes and Taylor, 1983)
18:1ω9/18:1ω7-ratio >1	Carnivore	(Graeve et al., 1997)
18:1ω9/18:1ω7-ratio <1	Suspension feeder	(Graeve et al., 1997)

22:5ω6 [Table 2, (Graeve et al., 2002; Perissinotto et al., 2007)]. Furthermore, 7-35% of total PLFAs in pyrosomes contained the dinoflagellate markers C18-PUFAs and C22-PUFAS. The 16:1ω7/16:0-ratio- and 20:5ω3/22:6ω3-ratio-values below 1 also suggest a dinoflagellate-dominated diet [Table 2, (Dalsgaard et al., 2003)]. Unfortunately, the PLFAs 18:1ω9 co-eluted with 18:1ω7, so that it could not specified whether the pyrosomes from the DISCOL site were mainly carnivores or suspension feeders. $\delta^{13}C_{FA}$ of the ten most abundant fatty acids in pyrosomes ranged from -44.4 ± 22.6‰ (EPA) to -17.2 ± 12.2‰ (adrenic acid) in tFAs, from -28.1 ± 1.17‰ (LA) to -9.28 ± 13.1‰ (arachidonic acid, ARA: 20:4ω6) in PLFAs, and from -29.8 ± 5.86‰ (stearic acid: 18:0) to -15.6 ± 11.1 ‰ (lignoceric acid: 24:0) in NLFAs (Table 1).

Biogeochemical composition of deep-sea surface sediments

Deep-sea surface sediments (0 – 2 cm sediment layer, n=29) in the surveyed region had a C content of 0.67 ± 0.08% C DM sediment^{-1} and a N content of 0.15 ± 0.02% N DM sediment^{-1}. The 2 – 5 cm sediment layer (n=28) had a C content of 0.62 ± 0.06% C DM sediment^{-1}, a N content of 0.14 ± 0.001% N DM sediment^{-1}. The resulting C/N-ratios were for both depth layers ~5.1.

The most abundant PLFAs in the deep-sea sediment were palmitoleic acid (16:1ω7*cis*) (0 – 2 cm sediment layer: 16:8 ± 0.64%) and behenic acid (22:0) (2 – 5 cm sediment layer: 14.1 ± 11.8%) (Table 1). $\delta^{13}C_{FA}$ of PLFAs varied from -19.8 ± 2.26‰ (oleic acid 18:1ω9*cis*, co-eluted with LA 18:2ω6*trans* and ALA) to -11.5 ± 3.05‰ (palmitic acid) in surface sediment (0 – 2 cm layer) and from -24.8 ± 0.69‰ (behenic acid) to -10.4 ± 1.28‰ (palmitoleic acid: 16:1ω7*cis*) in subsurface sediment (2 – 5 cm layer).

Carbon and nitrogen contribution of pyrosomes

Mean regional C and N contributions of pyrosomes in the entire surveyed region was 14 ± 41 mg C m^{-2} and 3.2 ± 10 mg N m^{-2} (range: 0 – 216 mg C m^{-2} and 0 – 51 mg N m^{-2}; n = 46). In the EBS transects, the average C and N deposition was more than 72 times higher (123 ± 79 mg C m^{-2} and 29 ± 18 mg N m^{-2}, range: 40 – 216 mg C m^{-2} and 9.4 – 51 mg N m^{-2}; n = 4) than in the areas with an undisturbed seafloor (1.7 ± 1.8 mg C m^{-2} and 0.40 ± 0.43 mg N m^{-2}, range: 0 – 6.3 mg C m^{-2} and 0 – 1.5 mg N m^{-2}; n = 26). The plough-disturbed seafloor had higher levels of pyrosome C (7.0 ± 16 mg C m^{-2} and 1.6 ± 3.8 mg N m^{-2}, range: 0 – 66 mg C m^{-2} and 0 – 15 mg N m^{-2}; n=16) than the undisturbed region, but lower than the EBS-disturbed region. This translates to an estimated rate of minimum 2.4 to maximum 20 mg C m^{-2} d^{-1} and of minimum 0.5 to maximum 4.6 mg N m^{-2} d^{-1} during the food fall event (assuming the removal rate of *Phacellaphora camtschatica* at 5,300 m water depth in the western Pacific: minimum 0.6 g wet mass (WM) d^{-1}, maximum 5.4 g WM d^{-1}; equivalent to 2.6 mg C d^{-1} and 21 mg C d^{-1} or 0.6 mg N d^{-1} and 5.0 mg N d^{-1} or 17% d^{-1} and 144% d^{-1}; Sweetman, unpublished data) compared to a total benthic C demand of 6 to 11 mg C m^{-2} d^{-1} in the DEA (Vonnahme et al., 2020).

Faunal associations

Overall, we observed 2,958 individual pyrosome carcasses on the seafloor with OFOS, 184 of which were observed in close proximity to other fauna including taxa of the phyla Echinodermata, Arthropoda and Cnidaria. Close up observations by ROV showed pyrosome colonies to be (putatively) consumed by anemones, brittle stars, seastars and isopods (Figure 5).

Additionally, OFOS and ROV observations showed white organisms inside the pyrosome carcasses, potentially amphipods.

Discussion

Our serendipitous observations of a pyrosome bloom in open ocean waters revealed a pathway for C and N from the photic to the abyssal zone. Our observations, which are among the deepest jelly falls to date, show that pyrosome fluxes may contribute significantly to the local carbon and nitrogen flux of the abyssal plain in the Peru Basin. Additionally, these carcasses provide essential fatty acids to diverse deep-sea scavengers. Temporal analysis showed a peak in seafloor counts approximately 29 days after the first pyrosome observation on the seafloor during the second cruise leg, as well as a gradual decrease in pyrosome carcasses on the seafloor after the peak. The accumulation of carcasses and their subsequent decrease was observed over a relatively broad area of the seafloor. This illustrates the relatively short period of the phenomenon and highlights the challenge associated with capturing biological events relevant to the carbon pump that are stochastic in space and time. Recently disturbed seafloor contained up to twofold higher carbon concentrations than undisturbed surrounding seafloor. While the biological effects of this accumulation require further research, our findings clearly illustrate the urgency for the consideration of pelagic-benthic coupling in the context of deep-sea benthic resource extraction management and impact assessments.

Pyrosomes in the Peru Basin

The pyrosomes collected at the DISCOL site grazed mainly on dinoflagellates as indicated by the specific PLFA ratios 16:1ω7/16:0 and 20:5ω3/22:6ω3 and on Prymnesiophyceae as revealed by the fatty acid markers oleic acid, moroctic acid, and 22:5ω6. *Pyrosoma atlanticum* from the Indian Ocean and the Northern California Current have a similar diet and consume predominantly dinoflagellates and Prymnesiophyceae as identified by their fatty acid profiles (Perissinotto et al., 2007; Schram et al., 2020). Additionally, lower concentrations of the calanoid copepod markers gondoic acid and 22:1ω11 in pyrosome tissue from the DISCOL site suggest that these pyrosomes may predate upon zooplankton or ingest their faeces. However, copepod contribution to the overall pyrosome diet is likely very small as implied by the isotope value of $\delta^{13}C$ = -22.0‰ and $\delta^{15}N$ = 2.59. Though the $\delta^{13}C$ value of the pyrosomes was in the range of the $\delta^{13}C$ value of mesozooplankton in the eastern tropical Pacific [range: -19.9 to -22.3‰ (Décima et al., 2019)], where sediment trap samples had a $\delta^{13}C$ value of -24.1‰ (Décima et al., 2019), the pyrosomes were depleted in ^{15}N compared to *Pyrosoma atlanticum* from the Central Arabian Sea [$\delta^{15}N$ = 7.43‰ (Gauns et al., 2015)] and from the Northern California Current [$\delta^{15}N$ = 7.5‰ (Schram et al., 2020)]. This indicates that pyrosomes in the present study had a lower trophic level compared to one in the other studies.

Pyrosome food falls linking epipelagic and abyssal plain food webs

The importance of pyrosomes as vectors of C and N to the deep sea, has been noted in several ocean basins (Kuo et al., 2015; Miller et al., 2019; Schram et al., 2020; Stenvers et al., 2021). Pyrosomes are particularly effective vectors because of efficient feeding and a combination of high fecal pellet production, daily vertical migration (Henschke et al., 2019) and rapidly sinking carcasses with high C content [up to 9% DM in the DISCOL area, but previously reported 35% – 38% DM in the South Atlantic and the Central Arabian Sea (Lebrato and Jones, 2009; Gauns et al., 2015)]. The observed pyrosome flux in the DISCOL area was lower than fluxes of pyrosomes and other gelatinous zooplankton reported in shallower areas in the South Atlantic (5 g C m^{-2} at 1,275 m)(Lebrato and Jones, 2009), but comparable to the C flux of pyrosomes off Cabo Verde [North-East Atlantic, 0.6 to 42 mg C m^{-2} (Stenvers et al., 2021)] and to the C flux of jelly falls in the North-East Pacific (*Salpa*, >30 mg C m^{-2} d^{-1} at 3,400 m)(Smith et al., 2018) and Norwegian fjords (*Periphylla*, 13 mg C m^{-2} d^{-1}) (Sweetman and Chapman, 2015). The pyrosome standing stock on the seafloor in the DISCOL region was likely contributing significantly to the regional carbon pump at the time of this study: The mean regional pyrosome C deposition observed during this study (14 mg C m^{-2}, ~2 to 20 mg C m^{-2} d^{-1} or 0.7 to 7 g C m^{-2} yr^{-1}) would equal 182 to 1543% of the flux of particulate organic C [1.3 mg C m^{-2} d^{-1} or 0.5 g C m^{-2} yr^{-1} calculated based on sediment porosity: 0.93 ± 0.01, sedimentation velocity: 0.4 cm kyr^{-1}, C content in 0-2 cm sediment layer: 0.67 ± 0.08% C DM $sediment^{-1}$(Haffert et al., 2020)] and 39 to 184% of the total respired benthic C flux [6 – 11 mg C m^{-2} d^{-1} or 2 – 4 g C m^{-2} yr^{-1} (Vonnahme et al., 2020)] in the DISCOL area. Furthermore, we hypothesize that the deposited pyrosomes may increase the so-called 'priming effect potential'. This potential describes short-term changes in mineralization of sedimentary organic matter after the addition of substances to sediments due to interactions between added substances and the natural element cycles (Kuzyakov et al., 2000; Bianchi, 2011) in the surface sediment. In the Peru Basin, the pyrosomes have a higher lability than the rather refractory sedimentary organic matter. This difference in reactivity is corroborated by the fact that pyrosome total fatty acids and PLFAs were dominated by labile HUFAs with notable contributions of PUFAs compared to more stable MUFAs and saturated fatty acids which comprised the majority of sedimentary fatty acids. This change in relative contribution of HUFAs and PUFAs indicates that more unsaturated fatty acids were preferentially taken up and degraded by organisms scavenging the pyrosome food fall. Hence, these fatty acids are important for organic C cycling in deep-sea sediments and deposition of pyrosomes may also stimulate the overall degradation of organic matter at the seafloor. The pyrosomes additionally provided small amounts of the 'essential' fatty acids LA and ALA. However, a short-term (i.e., weeks to months) contribution of 0.001 ± 0.001 mg C m^{-2} (range: 0 – 0.005 mg C m^{-2}) LA and ALA is equivalent to 0.3% of the LA and ALA stock in the upper 2 cm of surface sediment in the Peru Basin (0.48 ± 0.05 mg C m^{-2} LA and ALA; Table 1), so that rapidly deposited phytodetritus might provide a more important

source of these specific fatty acids at undisturbed sites. In comparison, at freshly-trawled and medium-disturbed sites, the stochastically occurring deposition of pyrosomes adds up to 0.10 ± 0.06 mg C m^{-2} and 0.006 ± 0.013 mg C m^{-2}, respectively, of LA and ALA (Table 1). At these disturbed sites, a short-term increase in these 'essential' fatty acids might attract mobile deposit feeders, such as holothurians. However, recolonization may be delayed due to reduced food availability. This was observed in the DISCOL area where holothurians recolonized the area, but at a slower pace than expected based on their mobility/moving speed (Stratmann et al., 2018b).

Particulate N flux in the Peru Basin was 0.29 mg N m^{-2} d^{-1} (calculated based on sediment porosity: 0.93 ± 0.01, sedimentation velocity: 0.4 cm kyr^{-1}, N content in 0-2 cm sediment layer: 0.14 ± 0.01% N DM $sediment^{-1}$). This is in the range of the total PN flux between 3,350 and 3,800 m water depth in the subarctic Pacific (0.4 to 3.2 mg N m^{-2} d^{-1}) (Haake et al., 1993; Wu et al., 1999), but two to three orders of magnitude higher than the PN flux at Station M in the North-East Pacific (57 to 165 mg N m^{-2} d^{-1}) (Gaye et al., 2009). A pyrosome flux of 0.5 to 4.6 mg N m^{-2} d^{-1} is thus significant (189 to 1601%) to the regional particulate nitrogen flux during the time of the food fall.

Seafloor disturbance and accumulation of detritus

Our study also provides supporting evidence for the effects of physical seafloor disturbances on organic C deposition on the abyssal seafloor. Fine-scale variations in seafloor morphology at the scale of decimeters, physical seafloor disturbance and increased roughness clearly influenced the distribution of deposited pyrosome carcasses and resulted in local accumulations of deposited organic material. This was particularly true for the disturbance by trawling with the EBS, which caused 15 – 20 cm deep marks with steep walls (Vonnahme et al., 2020), resulting in an accumulation of pyrosomes on one side of the track. This accumulation was potentially a result of transport by benthic currents and subsequent hydrodynamic entrapment. Tidal movements dominated current activity in the first half of the expedition (Greinert, 2015). During SO242/2, the bottom current was primarily flowing from the west and with relatively low velocity (3 – 5 cm s^{-1}). The accumulation of pyrosomes along the eastern side of the EBS disturbance tracks corresponded with this hypothesized entrapment, resulting from the prevailing current direction from the west. This may indicate that currents carry the pyrosomes along the seafloor in the bottom boundary waters until they are physically stopped by the track edge. On average, the density of pyrosomes was almost two orders of magnitude greater in the recent EBS deep disturbance marks compared to those observed across the undisturbed surrounding seafloor. Significantly higher pyrosome densities in disturbed areas than those observed elsewhere during the same survey days confirmed that seafloor morphology was the main reason for differences in pyrosome density. Such accumulations of pyrosomes have also been observed along the sides of pipelines and in depressions off West Africa (Lebrato and Jones, 2009; Lebrato et al., 2022) with salps also having been observed to accumulate in hollows and furrows on the NW Atlantic slope (Cacchione et al., 1978). In order to analyze pyrosome accumulation in disturbed seafloor areas we here pooled undisturbed seafloor areas that included areas with and without nodules. However, we also observed individual pyrosomes trapped against individual manganese nodules. Increased seafloor rugosity as a result of nodule presence may therefore also result in increased organic matter accumulation which may create locally enhanced organic matter availability, potentially attracting fauna and influencing biodiversity in nodule areas. It may also result in flow patterns that prevent the deposition of smaller carcasses. The natural ability of nodule areas to trap pelagic detrital matter needs further investigation.

Although the EBS tracks may be considered a significant disturbance, resulting in reduced biological activities and relatively low organic matter remineralization rates (de Jonge et al., 2020), the greater accumulation of pyrosomes inside the disturbed areas did not appear to be caused by reduced scavenging in these disturbed areas. Previous studies show that the biomass of scavengers and densities of decapods, which can rapidly consume carcasses, were unexpectedly higher inside the plough tracks compared to outside on the undisturbed seafloor (Simon-Lledó et al., 2019a; de Jonge et al., 2020), suggesting higher scavenging rates and shorter residence times would be more likely. Although we do not know the abundance and role of macrofaunal scavenging at DISCOL, the megafaunal scavengers may be responsible for considerable carcass consumption, as has been observed elsewhere (Sweetman et al., 2014). Exact scavenging rates, however, are unknown and directed experiments with known pyrosome carcass numbers deposited on the seafloor would be required to acquire this information. From shallow-water experiments it is known that organic-matter deposition is correlated to sediment surface structure and morphology (Yager et al., 1993) but such biogeochemical knowledge is largely absent for the abyssal plain. While the alteration in organic matter deposition from human-induced physical seafloor disturbances may persist for centuries to millennia (Haeckel et al., 2001; Haffert et al., 2020; Volz et al., 2020), it is not well known to what extent such local accumulation of organic matter may impact benthic communities, biodiversity and functioning. Observations of complete shifts from faunal to microbial C cycling processes and spikes in seafloor respiration around gelatinous zooplankton falls suggest functional changes are likely (Sweetman et al., 2016).

Outlook

The significant accumulation of pelagic detritus in high relief features of physically disturbed areas of seafloor represents a rarely considered additional impact of anthropogenic seafloor disturbances on benthic communities, with such physical disturbances likely to result from activities such as benthic trawling or polymetallic nodule mining. Further studies are needed to address how such impacts may alter (e.g. enhance or decrease) biodiversity or biogeochemical

functioning, and whether ecosystem functioning is negatively impacted. Although our observations and calculations were done on a relatively fine scale (1 – 10m), the accumulation of organic matter in anthropogenic tracks is relevant to other types of seafloor disturbance (e.g. dredging, laying of undersea cables and pipelines, shipwrecks, and in particular trawl-fishing) (Martín et al., 2014). Anthropogenic activities taking place on the seafloor are increasing worldwide. Hence, our results are relevant on a global scale. Additionally, the accumulation of pyrosomes in disturbed regions can be illustrative of the deposition of other items from the water column onto the seafloor, including other forms of organic matter, but also plastics and other litter. The accumulation of pelagic detritus and other material in seafloor areas that have lost their natural integrity is likely a general impact (i.e. not pyrosome bloom specific) that requires consideration in future trawling and deep-seabed mining management strategies, i.e. by design of comprehensive (nodule and fish) exploitation technologies. How these locally elevated organic matter accumulations may further impact these already disturbed environments is unknown, but is a relevant aspect of potential mining effects on the ecology of abyssal plains, or benthic trawling on shelf seas, seamounts, and ocean margins.

Data availability statement

Data on pyrosome observations is summarized and provided in Supplementary Table 1. Individual pyrosome annotations in relation to seafloor type will be available in: Purser, Autun; Hoving, Henk-Jan (2022), "Pyrosome corpse observations across the undisturbed and anthropogenically disturbed seafloor of the DISCOL experimental area, Peru Basin", Mendeley Data, V1, doi: 10.17632/6nyh68vtv9.1. Bathymetric data is available in PANGAEA at https://doi.org/10.1594/PANGAEA.905616 and https://doi.org/10.1594/PANGAEA.905579. Seafloor images are available in PANGAEA at https://doi.org/10.1594/PANGAEA.890634. Water column observations and biochemical data are uploaded in PANGAEA and the link will be made available after publication. Data from the biogeochemical analysis are found under the following links: Sediment: https://doi.org/10.1594/PANGAEA.905377. Sediment PLFA: https://doi.pangaea.de/10.1594/PANGAEA.946213. Pyrosome: https://doi.pangaea.de/10.1594/PANGAEA.946209. Pyrosome total fatty acid: https://doi.pangaea.de/10.1594/PANGAEA.946256. Pyrosome PLFA: https://doi.pangaea.de/10.1594/PANGAEA.946259. Pyrosome NLFA: https://doi.pangaea.de/10.1594/PANGAEA.946266.

Author contributions

JG, AB, AP, YM, IS, AS, KD, MH, TS, ES-L performed fieldwork. TS, AP, YM, IS, ES-L, KD, H-JH performed (lab and/or image) analysis. H-JH, AP, DJ and TS drafted the manuscript. All authors contributed to the article and approved the submitted version.

Funding

This research was funded by the German Ministry of Research (BMBF) in the framework of the MiningImpact project (grant no. 03F0707A-G) as part of the Joint Programming Initiative of Healthy and Productive Seas and Oceans (JPI Oceans). AB supported the expedition with her ERC AdvG ABYSS (294757) and received support from the Max Planck Society and the Helmholtz Association of German Research Centres (HGF). H-JH is funded by the DFG (Deutsche Forschungsgemeinschaft) under grant HO 5569/2-1 (Emmy Noether Junior Research Group). KD and AS were also supported by the Jellyfarm project funded through the Norwegian Research Council (Grant no. 244572). TS is funded by the Dutch Research Council (NWO) under NWO-Rubicon grant no. 019.182EN.012 and NWO-Talent program Veni grant no. VI.Veni.212.211. DJ, ES-L and AKS were supported by the UK Natural Environment Research Council Seabed Mining And Resilience To EXperimental impact (SMARTEX) project (Grant Reference NE/T003537/1).

Acknowledgments

We are indebted to the professional assistance of the captain and crew of RV SONNE during cruise SO242 and the GEOMAR team operating ROV Kiel 6000. Lammertjan Dam (Groningen University) is thanked for his help with statistical analysis. Julian Stauffer and Nis Hansen are acknowledged for help with Figure 2, Vanessa Stenvers for valuable input on a manuscript version.

Conflict of interest

The authors declare that the research was conducted in the absence of any commercial or financial relationships that could be construed as a potential conflict of interest.

Publisher's note

All claims expressed in this article are solely those of the authors and do not necessarily represent those of their affiliated organizations, or those of the publisher, the editors and the reviewers. Any product that may be evaluated in this article, or claim that may be made by its manufacturer, is not guaranteed or endorsed by the publisher.

Supplementary material

The Supplementary Material for this article can be found online at: https://www.frontiersin.org/articles/10.3389/fmars.2023.1192242/full#supplementary-material

References

Bernardino, A. F., Smith, C. R., Baco, A., Altamira, I., and Sumida, P. Y.G. (2010). Macrofaunal succession in sediments around kelp and wood falls in the deep NE pacific and community overlap with other reducing habitats. *Deep Sea Res. Part I: Oceanographic Res. Papers* 57 (5), 708–723. doi: 10.1016/j.dsr.2010.03.004

Bianchi, T. S. (2011). The role of terrestrially derived organic carbon in the coastal ocean: a changing paradigm and the priming effect. *Proc. Natl. Acad. Sci.* 108 (49), 19473–19481. doi: 10.1073/pnas.1202757109

Bligh, E. L. G., and Dyer, W. J. A. (1959). A rapid method of total lipid extraction and purification. *Can. J. Biochem. Physiol.* 37, 911–917. doi: 10.1139/o59-099

Bluhm, H. (2001). Re-establishment of an abyssal megabenthic community after experimental physical disturbance of the seafloor. *Deep-Sea Res. II* 48, 3841–3868. doi: 10.1016/S0967-0645(01)00070-4

Bluhm, H., Schriever, G., and Thiel, H. (1995). Megabenthic recolonization in an experimentally disturbed abyssal manganese nodule area. *Mar. Georesour. Geotechnol.* 13, 393–416. doi: 10.1080/10641199509388295

Boetius, A. (2015). *RV SONNE fahrtbericht / cruise report SO242-2 [SO242/2]: JPI OCEANS ecological aspects of deep-Sea mining, DISCOL revisited, guayaquil - guayaquil (Equador)* (Kiel, Germany: GEOMAR Helmholtz-Zentrum für Ozeanforschung). doi: 10.3289/GEOMAR_REP_NS_27_2015

Boetius, A., and Haeckel, M. (2018). Mind the seafloor. *Science* 359 (6371), 34. doi: 10.1126/science.aap7301

Boschker, H. (2008). Linking microbial community structure and functioning: stable isotope (13C) labeling in combination with PLFA analysis. *Mol. Microb. Ecol. Manual II*, 1673–1688. doi: 10.1007/978-1-4020-2177-0_807

Brodeur, R. D., Auth, T. D., and Phillips, A. J. (2019). Major shifts in pelagic micronekton and macrozooplankton community structure in an upwelling ecosystem related to an unprecedented marine heatwave. *Front. Mar. Sci.* 6, 212. doi: 10.3389/fmars.2019.00212

Burd, A. B., Hansell, D. A., Steinberg, D. K., Anderson, T. R., Arístegui, J., Baltar, F, et al. (2010). Assessing the apparent imbalance between geochemical and biochemical indicators of meso- and bathypelagic biological activity: what the @$#! is wrong with present calculations of carbon budgets? *Deep Sea Res. Part II: Topical Stud. Oceanogr.* 57 (16), 1557–1571. doi: 10.1016/j.dsr2.2010.02.022

Burdge, G. C., and Calder, P. C. (2014). Introduction to fatty acids and lipids. *World Rev. Nutr. Dietetics* 112, 1–16. doi: 10.1159/000365423

Cacchione, D., Rowe, G., and Malahoff, A. (1978). Submersible investigation of outer Hudson submarine canyon. *Sedimentation Submarine Canyons Fans Trenches*, 42–50.

Choy, C. A., Haddock, S. H. D., and Robison, B. H. (2017). Deep pelagic food web structure as revealed by *in situ* feeding observations. *Proc. R. Soc. B: Biol. Sci.* 284 (1868), 20172116. doi: 10.1098/rspb.2017.2116

Cornwall, W. (2019). Invasion of the glowing sea pickles. *Science* 363 (6426), 445. doi: 10.1126/science.363.6426.445

Dalsgaard, J., John, M., Kattner, G., Mueller-Navarra, D., and Hagen, W. (2003). Fatty acid trophic markers in the pelagic marine environment. *Adv. Mar. Biol.* 46, 225–340. doi: 10.1016/S0065-2881(03)46005-7

Décima, M., Stukel, M. R., López-López, L., Landry, M. R, et al. (2019). The unique ecological role of pyrosomes in the Eastern tropical pacific. *Limnol. Oceanogr.* 64 (2), 728–743. doi: 10.1002/lno.11071

de Jonge, D., Stratmann, T., Lins, L., Vanreusel, A., Purser, A., Marcon, Y., et al. (2020). Abyssal food-web model indicates faunal carbon flow recovery and impaired microbial loop 26 years after a sediment disturbance experiment. *Prog. In Oceanogr.* 189. doi: 10.1016/j.pocean.2020.102446

Durden, J., Bett, B., Jones, D., Huvenne, V., and and Ruhl, H. (2015). Abyssal hills – hidden source of increased habitat heterogeneity, benthic megafaunal biomass and diversity in the deep sea. *Prog. Oceanogr.* 162. doi: 10.1016/j.pocean.2015.06.006

Durden, J. M., Bett, B. J., Huffard, C. L., Pebody, C., Ruhl, H. A., and Smith, K. L. (2020). Response of deep-sea deposit-feeders to detrital inputs: a comparison of two abyssal time-series sites. *Deep Sea Res. Part II: Topical Stud. Oceanogr.* 173, 104677. doi: 10.1016/j.dsr2.2019.104677

Falk-Petersen, S., Sargent, J. R., and Tande, K. S. (1987) Lipid composition of zooplankton in relation to the Sub-Arctic food web. *1*. 8, 115–120.

Gage, J., Roberts, J., and Humphery, J. (2005). "Potential impacts of deep-sea trawling on the benthic ecosystem along the northern European continental margin: a review," in *American Fisheries Society Symposium*. Benthic Habitats and the Effects of Fishing (Tampa Florida: American Fisheries Society)

Gaillard, B., Meziane, T., Tremblay, R., Archambault, P., Blicher, M. E., Chauvaud, L., et al (2017). Food resources of the bivalve Astarte elliptica in a sub-Arctic fjord: a multi-biomarker approach. *Marine Ecology Progress Series*. 567, 139–156.

Gauns, M., Mochemadkar, S., Pratihary, A., Roy, R., Wajih, S., Naqvi, A., et al. (2015). Biogeochemistry and ecology of pyrosoma spinosum from the central Arabian Sea. *Zoological Stud.* 54 (JAN), 3. doi: 10.1186/s40555-014-0075-6

Gausepohl, F., Hennke, A., Schoening, T., Köser, K., and Greinert, J. (2020). Scars in the abyss: reconstructing sequence, location and temporal change of the 78 plough tracks of the 1989 DISCOL deep-sea disturbance experiment in the Peru basin. *Biogeosciences* 17 (6), 1463–1493. doi: 10.5194/bg-17-1463-2020

Gaye, B., Wiesner, M. G., and Lahajnar, N. (2009). Nitrogen sources in the south China Sea, as discerned from stable nitrogen isotopic ratios in rivers, sinking particles, and sediments. *Mar. Chem.* 114 (3–4), 72–85. doi: 10.1016/j.marchem.2009.04.003

Graeve, M., Kattner, G., Wiencke, C., and Karsten, U. (2002). Fatty acid composition of Arctic and Antarctic macroalgae: indicator of phylogenetic and trophic relationships. *Mar. Ecol. Prog. Serie* 231, 67–74. doi: 10.3354/meps231067

Graeve, M., Kattner, G., and Piepenburg, D. (1997). Lipids in Arctic benthos: does the fatty acid and alcohol composition reflect feeding and trophic interactions? *Polar Biology*. 18, 53–61.

Grassle, J. F., and Morse-Porteous, L. S. (1987). Macrofaunal colonization of disturbed deep-sea environments and the structure of deep-sea benthic communities. *Deep Sea Res. Part A. Oceanographic Res. Papers* 34 (12), 1911–1950. doi: 10.1016/0198-0149(87)90091-4

Greinert, J. (2015). *Cruise report SO242-1 [SO242/1]: JPI OCEANS ecological aspects of deep-Sea mining, DISCOL revisited, guayaquil - guayaquil (Equador)*. doi: 10.3289/GEOMAR_REP_NS_26_2015

Haake, B., Ittekkot, V., Honjo, S., and Manganini, S. (1993). Amino acid, hexosamine and carbohydrate fluxes to the deep subarctic pacific (Station p). *Deep-Sea Res. Part I* 40 (3), 547–560. doi: 10.1016/0967-0637(93)90145-S

Haeckel, M., König, I., Riech, V., Weber, M. E., and Suess, E. (2001). Pore water profiles and numerical modelling of biogeochemical processes in Peru basin deep-sea sediments. *Deep Sea Res. Part II: Topical Stud. Oceanogr.* 48 (17), 3713–3736. doi: 10.1016/S0967-0645(01)00064-9

Haffert, L., Haeckel, M., Stigter, H., and Janssen, F. (2020). Assessing the temporal scale of deep-sea mining impacts on sediment biogeochemistry. *Biogeosciences* 17, 2767–2789. doi: 10.5194/bg-17-2767-2020

Harris, P., Macmillan-Lawler, M., Rupp, J., and Baker, E. (2014). Geomorphology of the oceans. *Mar. Geol.* 352, 4–24. doi: 10.1016/j.margeo.2014.01.011

Hein, J., and Koschinsky, A. (2014). *Deep-ocean ferromanganese crusts and nodules', geochemistry of mineral deposits: treatise of geochemistry*, *2nd Edition*, Vol. 13. 273–291.

Henschke, N., Pakhomov, E. A., Kwong, L. E., Everett, J. D., Laiolo, L., Coghlan, A. R., et al. (2019). Large Vertical migrations of pyrosoma atlanticum play an important role in active carbon transport. *J. Geophys. Res.: Biogeosci.* 124 (5), 1056–1070. doi: 10.1029/2018JG004918

Higgs, N. D., Gates, A. R., and Jones, D. O. B. (2014). Fish food in the deep Sea: revisiting the role of Large food-falls. *PloS One* 9 (5), e96016. doi: 10.1371/journal.pone.0096016

Jeffries, H. P. (1970). Seasonal composition of temperate plankton communities: fatty acids. *Limnol and Oceanogr.* 15 (3), 419–426.

Jones, E., Collins, M., Bagley, P., Addison, S., and Priede, I. (1998). The fate of cetacean carcasses in the deep sea: observations on consumption rates and succession of scavenging species in the abyssal north-east Atlantic ocean. *Proc. R. Soc. B: Biol. Sci.* 265, 1119–1127. doi: 10.1098/rspb.1998.0407

Kelly, J. R., and Scheibling, R. E. (2012) Fatty acids as dietary tracers in benthic food webs. *Mar. Ecol. Prog. Ser.* 446, 1–22. doi: 10.3354/meps09559

König, I., Haeckel, M., Lougear, A., Suess, E., and Trautwein, A. (2001). A geochemical model of the Peru basin deep-sea floor - and the response of the system to technical impacts. *Deep Sea Res. Part II: Topical Stud. Oceanogr.* 48, 3737–3756. doi: 10.1016/S0967-0645(01)00065-0

Kuo, C., Fan, T.-Y., Li, H.-H., Lin, C.-W., Liu, L.-L., and Kuo, F. (2015). An unusual bloom of the tunicate, pyrosoma atlanticum , in southern Taiwan. *Bull. Mar. Sci.* 91, 363–364. doi: 10.5343/bms.2014.1090

Kuzyakov, Y., Friedel, J. K., and Stahr, K. (2000). Review of mechanisms and quantification of priming effects. *Soil Biol. Biochem.* 32 (11), 1485–1498. doi: 10.1016/S0038-0717(00)00084-5

Lebrato, M., Pahlow, M., Frost, J. R., Küter, M., de Jesus Mendes, P., Molinero, J.-C., et al. (2019). Sinking of gelatinous zooplankton biomass increases deep carbon transfer efficiency globally. *Global Biogeochem. Cycles* 33 (12), 1764–1783. doi: 10.1029/2019GB006265

Lebrato, M., Molinero, J. -C., Mychek-Londer, J. G., Gonzalez, E. M., and Jones, D. O. B. (2022). Gelatinous carbon impacts benthic megafaunal communities in a continental margin. *Front. Mar. Sci.* doi: 10.3389/fmars.2022.902674

Léveillé, J. C., Amblard, C., and Bourdier, G. (1997). Fatty acids as specific algal markers in a natural lacustrian phytoplankton. *J. Plankton Res.* 19, 469–490. doi: 10.1093/plankt/19.4.469

Lebrato, M., and Jones, D. O. B. (2009). Mass deposition event of pyrosoma atlanticum carcasses off ivory coast (West Africa). *Limnol. Oceanogr.* 54 (4), 1197–1209. doi: 10.4319/lo.2009.54.4.1197

Lucas, C. H., Jones, D. O.B., Hollyhead, C. J., Condon, R. H., Duarte, C. M., Graham, W. M., et al. (2014). Gelatinous zooplankton biomass in the global oceans: geographic variation and environmental drivers. *Global Ecol. Biogeogr.* 23 (7), 701–714. doi: 10.1111/geb.12169

Luo, J. Y., Condon, R. H., Stock, C. A., Duarte, C. M., Lucas, C. H., Pitt, K. A., et al. (2020). Gelatinous zooplankton-mediated carbon flows in the global oceans: a data-driven modeling study. *Global Biogeochem. Cycles* 34 (9), e2020GB006704. doi: 10.1029/2020GB006704

Marcon, Y., and Purser, A. (2017). PAPARA(ZZ)I: an open-source software interface for annotating photographs of the deep-sea. *SoftwareX* 6, 69–80. doi: 10.1016/j.softx.2017.02.002

Martín, J., Puig, P., Masqué, P., Palanques, A., and Sánchez-Gómez, A. (2014). Impact of bottom trawling on deep-Sea sediment properties along the flanks of a submarine canyon. *PloS One* 9 (8), e104536. doi: 10.1371/journal.pone.0104536

Mayzaud, P., Chanut, J., and Ackman, R. (1989). Seasonal changes of the biochemical composition of marine particulate matter with special reference to fatty acids and sterols. *Marine Ecology Progress Series*. 56 (1), 189–204. doi: 10.3354/meps056189

Miller, R. R., Santora, J. A., Auth, T. D., Sakuma, K. M., Wells, B. K., Field, J. C., et al. (2019). *Distribution of pelagic thaliaceans, thetys vagina and pyrosoma atlanticum, during a period of mass occurrence within the California current, CalCOFI report*.

O'Loughlin, J. H., Bernard, K. S., Daly, E. A., Zeman, S., Fisher, J. L., Brodeur, R. D., et al. (2020). Implications of pyrosoma atlanticum range expansion on phytoplankton standing stocks in the northern California current. *Prog. Oceanogr.* 188, 102424. doi: 10.1016/j.pocean.2020.102424

Parkes, R. J., and Taylor, J. (1983). The relationship between fatty acid distributions and bacterial respiratory types in contemporary marine sediments. *Estuarine, Coastal and Shelf Science*. 16, 173–189. doi: 10.1016/0272-7714(83)90139-7

Paul, S. A. L., Haeckel, M., Bau, M., Bajracharya, R., Koschinsky, A., et al. (2019). Small-scale heterogeneity of trace metals including rare earth elements and yttrium in deep-sea sediments and porewaters of the Peru basin, southeastern equatorial pacific. *Biogeosciences* 16 (24), 4829–4849. doi: 10.5194/bg-16-4829-2019

Perissinotto, R., Mayzaud, P., Nichols, P. D., and Labat, J. P. (2007). Grazing by pyrosoma atlanticum (Tunicata, thaliacea) in the south Indian ocean. *Mar. Ecol. Prog. Ser.* 330, 1–11. doi: 10.3354/meps330001

Pond, D., Dixon, D., Bell, M., Fallick, A. E., and Sargent, J. (1997). Occurrence of 16:2 (n-4) and 18:2(n-4) fatty acids in the lipids of the hydrothermal vent shrimps rimicaris exoculata and alvinocaris markensis: nutritional and trophic implications. *Mar. Ecol. Prog. Ser.* 156, 167–174. doi: 10.3354/meps156167

Pond, D., Allen, C., Bell, M., Dover, C., Fallick, A. E., and Dixon, D. (2002). On the origins of long-chain, polyunsaturated fatty acids in the hydrothermal vent worms, ridgea piscesae and protis hydrothermica. *Mar. Ecol. Prog. Ser.* 225, 219–226. doi: 10.3354/meps225219

Ramirez-Llodra, E., Brandt, A., Danovaro, R., De Mol, B., Escobar, E., German, C. R., et al. (2010). Deep, diverse and definitely different: unique attributes of the world's largest ecosystem. *Biogeosciences* 7 (9), 2851–2899. doi: 10.5194/bg-7-2851-2010

Robison, B. (2004). Deep pelagic biology. *J. Exp. Mar. Biol. Ecol.* 300, 253–272. doi: 10.1016/j.jembe.2004.01.012

Robison, B. H., Reisenbichler, K. R., and Sherlock, R. E. (2005). Giant larvacean houses: rapid carbon transport to the deep Sea floor. *Science* 308 (5728), 1609 LP–1611. doi: 10.1126/science.1109104

Sakuma, K. M., Field, J. C., Mantua, N. J., Ralston, S., Marinovic, B. B., and Carrion, C. N. (2016). Anomalous epipelagic micronekton assemblage patterns in the neritic waters of the California current in spring 2015 during a period of extreme ocean conditions. *CalCOFI Report*. 57, 163–183.

Sala, E., Mayorga, J., Bradley, D., Cabral, R. B., Atwood, T. B., Auber, A., et al. (2021). Protecting the global ocean for biodiversity, food and climate. *Nature* 592 (7854), 397–402. doi: 10.1038/s41586-021-03371-z

Schram, J., Sorensen, H. L., Brodeur, R. D., Galloway, A., and Sutherland, K. (2020). Abundance, distribution, and feeding ecology of pyrosoma atlanticum in the northern California current. *Mar. Ecol. Prog. Ser*. 651, 97–110. doi: 10.3354/meps13465

Simon-Lledó, E., Bett, B. J., Huvenne, V. A.I., Köser, K., Schoening, T., Greinert, J., et al. (2019a). Biological effects 26 years after simulated deep-sea mining. *Sci. Rep.* 9 (1), 8040. doi: 10.1038/s41598-019-44492-w

Simon-Lledó, E., Bett, B., Huvenne, V., Schoening, T., Benoist, N., and Jones, D. (2019b). Ecology of a polymetallic nodule occurrence gradient: implications for deep-sea mining. *Limnol. Oceanogr.* 64, 1883–1894. doi: 10.1002/lno.11157

Simon-Lledó, E., Bett, B., Huvenne, V., Schoening, T., Benoist, N., and Jeffreys, R. (2018). Megafaunal variation in the abyssal landscape of the clarion clipperton zone. *Prog. Oceanogr.* 170, 119–133. doi: 10.1016/j.pocean.2018.11.003

Simon-Lledó, E., Bett, B., Huvenne, V., Schoening, T., Benoist, N., Jeffreys, R., et al. (2020). Multi-scale variations in invertebrate and fish megafauna in the mid-eastern clarion clipperton zone. *Prog. Oceanogr.* 187, 102405. doi: 10.1016/j.pocean.2020.102405

Skerratt, J. H., Nichols, P. D., McMeekin, T. A., and Burton, H. (1995). Seasonal and inter-annual changes in planktonic biomass and community structure in eastern Antarctica using signature lipids. *Marine Chemistry*. 51, 93–113.

Smith, C. R., De Leo, F. C., Bernardino, A. F., Sweetman, A. K., and Arbizu, P. M. (2008). Abyssal food limitation, ecosystem structure and climate change. *Trends Ecol. Evol.* 23 (9), 518–528. doi: 10.1016/j.tree.2008.05.002

Smith, K. L., Ruhl, H. A., Kahru, M., Huffard, C. L., Sherman, A. D., et al. (2013). Deep ocean communities impacted by changing climate over 24 y in the abyssal northeast pacific ocean. *Proc. Natl. Acad. Sci.* 110 (49), 19838 LP–19841. doi: 10.1073/pnas.1315447110

Smith, K. L. Jr., Sherman, A. D., Huffard, C. L., McGill, P. R., Henthorn, R., Von Thun, S., et al. (2014). Large Salp bloom export from the upper ocean and benthic community response in the abyssal northeast pacific: day to week resolution. *Limnol. Oceanogr.* 59 (3), 745–757. doi: 10.4319/lo.2014.59.3.0745

Smith, K. L., Ruhl, H. A., Huffard, C. L., Messié, M., and Kahru, M. (2018). Episodic organic carbon fluxes from surface ocean to abyssal depths during long-term monitoring in NE pacific. *Proc. Natl. Acad. Sci.* 115 (48), 12235 LP–12240. doi: 10.1073/pnas.1814559115

Smith, K. L., and Kaufmann, R. (1999). Long-term discrepancy between food supply and demand in the deep Eastern north pacific. *Sci. (New York N.Y.)* 284, 1174–1177. doi: 10.1126/science.284.5417.1174

Snelgrove, P., Grassle, J. F., and Petrecca, R. (1994). Macrofaunal response to artificial enrichments and depressions in a deep-sea habitat. *J. Mar. Res.* 52, 345–369. doi: 10.1357/0022240943077082

Soltwedel, T., Bauerfeind, E., Bergmann, M., Bracher, A., Budaeva, N., Busch, K., et al. (2016). Natural variability or anthropogenically-induced variation? insights from 15 years of multidisciplinary observations at the arctic marine LTER site HAUSGARTEN. *Ecol. Indic.* 65, 89–102. doi: 10.1016/j.ecolind.2015.10.001

Stenvers, V. I., Hauss, H., Osborn, K. J., Neitzel, P., Merten, V., Scheer, S., et al. (2021). Distribution, associations and role in the biological carbon pump of pyrosoma atlanticum (Tunicata, thaliacea) off cabo Verde, NE Atlantic. *Sci. Rep.* 11 (1), 9231. doi: 10.1038/s41598-021-88208-5

Stockton, W. L., and DeLaca, T. E. (1982). Food falls in the deep sea: occurrence, quality, and significance. *Deep Sea Res. Part A. Oceanographic Res. Papers* 29 (2), 157–169. doi: 10.1016/0198-0149(82)90106-6

Stratmann, T., Soetaert, K., Kersken, D., and Van Oevelen, D. (2021). Polymetallic nodules are essential for food-web integrity of a prospective deep-seabed mining area in pacific abyssal plains. *Sci. Rep.* 11, 12238. doi: 10.1038/s41598-021-91703-4

Stratmann, T., Mevenkamp, L., Sweetman, A. K., Vanreusel, A., and van Oevelen, D. (2018a). Has phytodetritus processing by an abyssal soft-sediment community recovered 26 years after an experimental disturbance? *Front. Mar. Sci.* 5 (February). doi: 10.3389/fmars.2018.00059

Stratmann, T., Voorsmit, I., Gebruk, A., Brown, A., Purser, A., Marcon, Y., et al. (2018b). Recovery of holothuroidea population density, community composition, and respiration activity after a deep-sea disturbance experiment. *Limnol. Oceanogr.* 63 (5), 2140–2153. doi: 10.1002/lno.10929

Sutherland, K. R., et al. (2018). Range expansion of tropical pyrosomes in the northeast pacific ocean. *Ecology* 99 (10), 2397–2399. doi: 10.1002/ecy.2429

Sweetman, A., and Chapman, A. (2015). First assessment of flux rates of jellyfish carcasses (jelly-falls) to the benthos reveals the importance of gelatinous material for biological c-cycling in jellyfish-dominated ecosystems. *Front. Mar. Sci.* 2, 47. doi: 10.3389/fmars.2015.00047

Sweetman, A. K., Smith, C. R., Dale, T., and Jones, D. O. B. (2014). Rapid scavenging of jellyfish carcasses reveals the importance of gelatinous material to deep-sea food webs. *Proc. R. Soc. B: Biol. Sci.* 281 (1796), 20142210. doi: 10.1098/rspb.2014.2210

Sweetman, A., Chelsky, A., Pitt, K., Andrade, H., Oevelen, D., and Renaud, P. (2016). Jellyfish decomposition at the seafloor rapidly alters biogeochemical cycling and carbon flow through benthic food-webs. *Limnol. Oceanogr.* 61, 1449–1461. doi: 10.1002/lno.10310

Sweetman, A. K., Thurber, A. R., Smith, C. R., Levin, L. A., Mora, C., Wei, C.-L., et al (2017). "Major impacts of climate change on deep-sea benthic ecosystems," in *Elementa: science of the anthropocene*, vol. 5 . Eds. J. W. Deming and L. Thomsen doi: 10.1525/elementa.203

Thiel, H. (1991). From MESEDA to DISCOL: a new approach to deep-sea mining risk assessments. *Mar. Min.* 10, 369–386. doi: 10.1016/S0967-0645(01)00071-6

Thiel, H., Schriever, G., Ahnert, A., Bluhm, H., Borowski, C., and Vopel, K. (2001). The large-scale environmental impact experiment DISCOL–reflection and foresight. *Deep Sea Res. Part II: Topical Stud. Oceanogr.* 48 (17), 3869–3882. doi: 10.1016/S0967-0645(01)00071-6

Thiel, H., and Schriever, G. (1989). *Cruise report DISCOL 1, sonne cruise 61, Balboa/Panama - Callao/Peru 02.02. - 05.03.1989, Callao/Peru - Callao/Peru 07.03. - 03.04.1989* (Hamburg: Institut für Hydrobiologie und Fischereiwissenschaft, Universität Hamburg). doi: 10.2312/cr_so61

Thurber, A. R., Sweetman, A. K., Narayanaswamy, B. E., Jones, D. O.B., Ingels, J., and Hansman, R. L. (2014). Ecosystem function and services provided by the deep sea. *Biogeosciences* 11 (14), 3941–3963. doi: 10.5194/bg-11-3941-2014

Treude, T., Smith, C., Wenzhoefer, F., Carney, E., Bernardino, A., Hannides, A., et al. (2009). Biogeochemistry of a deep-sea whale fall: sulfate reduction, sulfide efflux and methanogenesis. *Mar. Ecol. Progress Ser. Mar. ECOL-PROGR Ser.* 382, 1–21. doi: 10.3354/meps07972

Van Cappellen, P. (2003). Biomineralization and global biogeochemical cycles. *Rev. Mineralogy Geochem.* 54, 357–381. doi: 10.2113/0540357

Vanreusel, A., Hilario, A., Ribeiro, P. A., Menot, L., and Arbizu, P. M. (2016). Threatened by mining, polymetallic nodules are required to preserve abyssal epifauna. *Sci. Rep.* 6 (1), 26808. doi: 10.1038/srep26808

van Soest, R. W. M. (1981). A monograph of the order pyrosomatida (Tunicata, thaliacea). *J. Plankton Res.* 3 (4), 603–631. doi: 10.1093/plankt/3.4.603

Volz, J. B., Haffert, L., Haeckel, M., Koschinsky, A., and Kasten, S. (2020). Impact of small-scale disturbances on geochemical conditions, biogeochemical processes and element fluxes in surface sediments of the eastern clarion–clipperton zone, pacific ocean. *Biogeosciences* 17 (4), 1113–1131. doi: 10.5194/bg-17-1113-2020

Vonnahme, T. R., Molari, M., Janssen, F., Wenzhöfer, F., Haeckel, M., Titschack, J., et al. (2020). Effects of a deep-sea mining experiment on seafloor microbial communities and functions after 26 years. *Sci. Adv.* 6 (18), eaaz5922. doi: 10.1126/sciadv.aaz5922

Wu, J., Calvert, S. E., Wong, C. S., and Whitney, F. A. (1999). Carbon and nitrogen isotopic composition of sedimenting particulate material at station papa in the subarctic northeast pacific. *Deep-Sea Res. Part II: Topical Stud. Oceanogr.* 46 (11–12), 2793–2832. doi: 10.1016/S0967-0645(99)00084-3

Yager, P., Nowell, A., and Jumars, P. (1993). Enhanced deposition to pits: a local food source for benthos. *J. Mar. Res.* 51, 209–236. doi: 10.1357/0022240933223819